ANTIBIOTICS

Deep learning–enabled discovery of antibiotics effective against *Neisseria gonorrhoeae*

Melis N. Anahtar[1,2,3,4]†, Jacqueline A. Valeri[1,3,4]†, Seyed Majed Modaresi[1,3,4]†, Aarti Krishnan[1,3,4,5], Nina M. Donghia[3], Samantha G. Palace[6], Erica J. Zheng[1,3,7], Aakanksha Gulati[3], Alicia Jorgenson[3], Abidemi Junaid[3], Parijat Bandyopadhyay[1,4], Andreas Luttens[1,4], Krishna Suresh[8], Paige Edwards[1,4], Felix Wong[1,4,9], Yu Zhang[1,3,4], Danilo Ritz[10], Margaux Gaborieau[11], Edmund Loh[11,12], Massimiliano Gaetani[13,14], Marie-Stephanie Aschtgen[11], Amir Ata Saei[11], Yonatan H. Grad[6], Donald E. Ingber[3,15,16], James J. Collins[1,3,4]*

Neisseria gonorrhoeae **is a common Gram-negative pathogen with increasing resistance to all recommended antibiotics. There is a critical need to improve the efficiency of the antibiotic hit discovery process to replenish the drug development pipeline. Here, we show that deep learning models can augment high-throughput screens to identify readily available molecules with narrow-spectrum activity against difficult-to-treat strains of *N. gonorrhoeae*. We phenotypically tested 38,650 small molecules for *N. gonorrhoeae* growth inhibition to train a predictive graph neural network (GNN) model. We benchmarked the model's performance against other architectures, including a large language model, and found that GNNs more accurately identify active, drug-like molecules that are structurally distinct from the training set and known antibiotics. Using the model to virtually screen ~6 million compounds, we identified 213 compounds for experimental validation and found that 83 (39%) inhibited *N. gonorrhoeae* growth. Two of these compounds were structurally dissimilar to existing antibiotics, maintained potency against multidrug-resistant *N. gonorrhoeae* strains in vitro, exhibited promising selectivity indices, and were rapidly bactericidal with low frequencies of resistance. Proteomic studies revealed their distinct mechanisms of action, with one compound targeting alanine racemase, an enzyme involved in the essential process of peptidoglycan synthesis. Furthermore, the compounds showed early promise in reducing *N. gonorrhoeae* titers in a human vagina-on-a-chip infection model and a mouse vaginal infection model. Our work establishes the deep learning–enabled discovery of selective antibacterial compounds against *N. gonorrhoeae* as a much-needed hit discovery tool to address the growing crisis of antimicrobial resistance for this pathogen.**

INTRODUCTION

Neisseria gonorrhoeae is a sexually transmitted Gram-negative bacterium that is one of the most urgent antibiotic-resistant threats to human health, according to the US Centers for Disease Control and Prevention (CDC) and the World Health Organization (*1*). Gonorrhea infection poses serious risks, such as increased HIV acquisition, infertility, infant blindness, and potentially life-threatening disseminated infection, if left untreated because of missed diagnosis or inadequate treatment (*2*). Previous empiric first-line therapies for gonorrhea—including penicillin, tetracycline, ciprofloxacin, cefixime, and azithromycin among others—are no longer recommended monotherapies because of excessively high resistance rates in circulating strains (*3*). The last remaining first-line monotherapy, ceftriaxone, is at risk of becoming obsolete, with resistance rates of >10% in parts of the world, mostly because of the dissemination of isolates with the *penA*60 allele (*4*). Emerging strains that are no longer susceptible to any recommended antibiotics have been identified in the US, Europe, and Asia-Pacific (*5*).

Faced with the threat of untreatable gonorrhea, new antibiotics are urgently needed. Gepotidacin and zoliflodacin, which target bacterial topoisomerases via orthogonal mechanisms to those of fluoroquinolones, earned US Food and Drug Administration (FDA) approval for treating urogenital gonorrhea in 2025 (*6*, *7*). Preexisting resistance to these antibiotics is extremely rare at present, but multiple missense mutations decrease their potency, calling their longevity as monotherapies into question (*8*). There is a critical need to fill the trickling antimicrobial development pipeline with promising antibiotic candidates, especially ones with distinct mechanisms of action.

Modern antimicrobial hit discovery has been performed using high-throughput screening (HTS), whereby large chemical libraries are tested for either inhibition of a particular target or inhibition of the growth of whole bacterial cells. Whole-cell or phenotypic HTS is advantageous for selecting compounds that can access their target (e.g., penetrate the outer membrane of Gram-negative bacteria) and retain efficacy in the complex milieu of a growing bacterial cell. Phenotypic HTS can also identify compounds with new mechanisms of

[1]Infectious Disease and Microbiome Program, Broad Institute of MIT and Harvard, Cambridge, MA 02142, USA. [2]Departments of Pathology and Medicine, Massachusetts General Hospital, Boston, MA 02114, USA. [3]Wyss Institute for Biologically Inspired Engineering, Harvard University, Boston, MA 02215, USA. [4]Institute for Medical Engineering and Science and Department of Biological Engineering, Massachusetts Institute of Technology, Cambridge, MA 02139, USA. [5]Whitehead Institute for Biomedical Research, Cambridge, MA 02142, USA. [6]Department of Immunology and Infectious Diseases, Harvard T. H. Chan School of Public Health, Boston, MA 02115, USA. [7]Program in Chemical Biology, Harvard University, Cambridge, MA 02138, USA. [8]Harvard Medical School, Boston, MA 02115, USA. [9]Integrated Biosciences Inc., Redwood City, CA 94065, USA. [10]Proteomics Core Facility, Biozentrum, University of Basel, Basel CH-4056, Switzerland. [11]Department of Microbiology, Tumor, and Cell Biology, Karolinska Institute, 171 77 Stockholm, Sweden. [12]Clinical Microbiology, Karolinska University Hospital, 171 76 Stockholm, Sweden. [13]Division of Chemistry I, Department of Medical Biochemistry and Biophysics, Karolinska Institute, 17 177 Stockholm, Sweden. [14]Chemical Proteomics Unit, Science for Life Laboratory (SciLifeLab), 171 77 Stockholm, Sweden. [15]Vascular Biology Program and Department of Surgery, Boston Children's Hospital and Harvard Medical School, Boston, MA 02115, USA. [16]Harvard John A. Paulson School of Engineering and Applied Sciences, Cambridge, MA 02539, USA.
†These authors contributed equally to this work.
*Corresponding author. Email: jimjc@mit.edu

action, although the mechanism can be difficult to ascertain and nonselective toxicity must be ruled out (*9*). Regardless of the HTS approach, it is practically infeasible to rely exclusively on physically screening compounds at a pace that keeps up with the recent growth in the make-on-demand chemical space, which now comprises more than 75 billion compounds (*10*).

Deep learning (DL) has recently been used to enrich antibiotic discovery efforts and is uniquely poised to benefit from the expansion of chemical libraries (*11*–*13*). DL is a subset of machine learning that uses artificial neural networks with multiple layers to automatically learn representations of data. DL extends the power of traditional structure-activity relationship (SAR) modeling by providing more flexible and automated ways to process and learn from raw or minimally processed molecular fingerprints, which are numerical representations of chemical structures (*14*). For example, DL-based models can identify higher-order, nonlinear interactions between molecular features encoded in a fingerprint, such as subtle interactions between atoms, functional groups, and molecular configurations that traditional methods miss, thereby improving predictive accuracy for tasks such as activity prediction or compound prioritization. Recent advances in large language models (LLMs) and diffusion models have also demonstrated potential in chemical property prediction and molecular generation (*15*). These approaches, alongside simpler models like random forests (RFs) and support vector machines (SVMs), highlight the diversity and power of DL in modern drug discovery, offering complementary methods for navigating vast chemical spaces.

Upon experimentally testing a small-to-medium-sized (10^3 to 10^4 compounds) library against a bacterial strain or protein target, the resulting dataset can be used to train DL models that predict properties of compounds in larger libraries of physically available or virtual, make-on-demand molecules. Highly scored compounds can be curated and experimentally validated as an efficient alternative to physically screening the entire compound library, in which typically only 0.5 to 5% of compounds have the desired activity (*11*, *13*, *16*). Graph neural networks (GNNs) represent molecules as graphs and learn structural representations directly, bypassing predefined fingerprints (*17*). The resulting vector representations can be combined with global molecular features and used to train models that virtually screen thousands of molecules per second. Here, we sought to train, evaluate, and implement GNNs to efficiently screen chemical space for small molecules with antibacterial activity against *N. gonorrhoeae*.

RESULTS

An experimental screen identifies compounds active against *N. gonorrhoeae*

We hypothesized that a DL model trained on phenotypic growth inhibition data for *N. gonorrhoeae* can identify compounds that specifically target this organism via orthogonal mechanisms of action from commonly used antimicrobials, thereby maintaining efficacy against drug-resistant strains (Fig. 1A). To test this hypothesis, we developed a training dataset by phenotypically screening chemical libraries for growth inhibition of *N. gonorrhoeae*. We first screened the Pharmakon library of 1755 clinically approved drugs (in 1760 unique formulations, "Pharmakon-1.7K"), which includes all first- and second-line antibiotics used for *N. gonorrhoeae* treatment. Each drug was tested in duplicate at a 50-μM final concentration in optically transparent Graver Wade medium with *N. gonorrhoeae* American Type Culture Collection (ATCC) 49226 (fig. S1A). ATCC 49226, a generally antibiotic-susceptible reference strain, was chosen over more drug-resistant strains to yield a larger number of active hits for model training. Because of *N. gonorrhoeae*'s lower maximal growth density relative to other common pathogens, bacterial growth was measured after 24 hours of incubation by optical density at 600 nm (OD_{600}) and a resazurin-based cell viability dye (PrestoBlue High Sensitivity) (*18*, *19*), which had a 25-fold higher signal-to-noise ratio than OD_{600} (Fig. 1B and fig. S1B). The growth inhibitory data were binarized (Fig. 1C). This resulted in 340 hits (19.3% hit rate), of which 126 were known antibacterials, 74 were other known anti-infectives, and the remaining 140 were non–anti-infective drugs (e.g., antidepressants, antipsychotics, and anti-inflammatories), which may act through distinct mechanisms of action from those of known antibiotics (Fig. 1D and data file S1) (*20*). Thus, screening the Pharmakon-1.7K library enabled the validation of our HTS approach, identified existing drugs with unintended antigonococcal activity, and provided training data on pharmaceutically acceptable small molecules.

To expand our training set beyond known drugs, we proceeded to test a much larger and structurally diverse library comprising 36,895 small molecules ("Internal-37K"; Fig. 2A and data file S1) for growth inhibitory activity against *N. gonorrhoeae* ATCC 49226. After binarization based on growth inhibitory activity (fig. S1C), the overall hit rate of the Internal-37K library was 2.5%, reflecting its relative diversity and dearth of known antibiotics compared with the Pharmakon-1.7K (Fig. 2B). There were many hits in the Internal-37K library that extended beyond known antibiotics, with 74% of the 929 hits containing a unique Murcko scaffold (table S1), indicating that we were exploring structurally distinct antimicrobial space. We combined the deduplicated Pharmakon-1.7K and Internal-37K datasets for subsequent model training and testing.

A directed message-passing GNN achieves superior predictive accuracy for antimicrobial activity against *N. gonorrhoeae*

We next compared the performances of three property-predicting DL models: (i) a directed message-passing GNN (D-MPNN; implemented via Chemprop, Fig. 2C) (*17*), (ii) an attention-based GNN [Attentive Fingerprint (Attentive FP)] (*21*), and (iii) a large chemical language model (ChemBERTa) (*15*) that had been pretrained on text representations of hundreds of thousands of molecules. The two GNNs, D-MPNN and Attentive FP, were chosen on the basis of their ability to accurately predict antibacterial activity against other organisms (*11*–*13*) or molecular properties in the Therapeutic Data Commons (*22*), respectively. ChemBERTa was selected because of the success and popularity of LLMs, such as ChatGPT and Gemini, and its reported equal if not better performance compared with D-MPNNs (*15*, *23*). We benchmarked these more complex models against simpler models that use a chemical fingerprint as input. Details of the model architectures and hyperparameter optimization are described in the Materials and Methods and table S2. For each model architecture, we evaluated the highest-performing model from hyperparameter optimization and found that the D-MPNN model had the highest area under the precision-recall curve (AUPRC), which is a more relevant metric than area under the receiver operating characteristic curve (AUROC) given the class imbalance with 97% of data points classified as a nonhit (table S3).

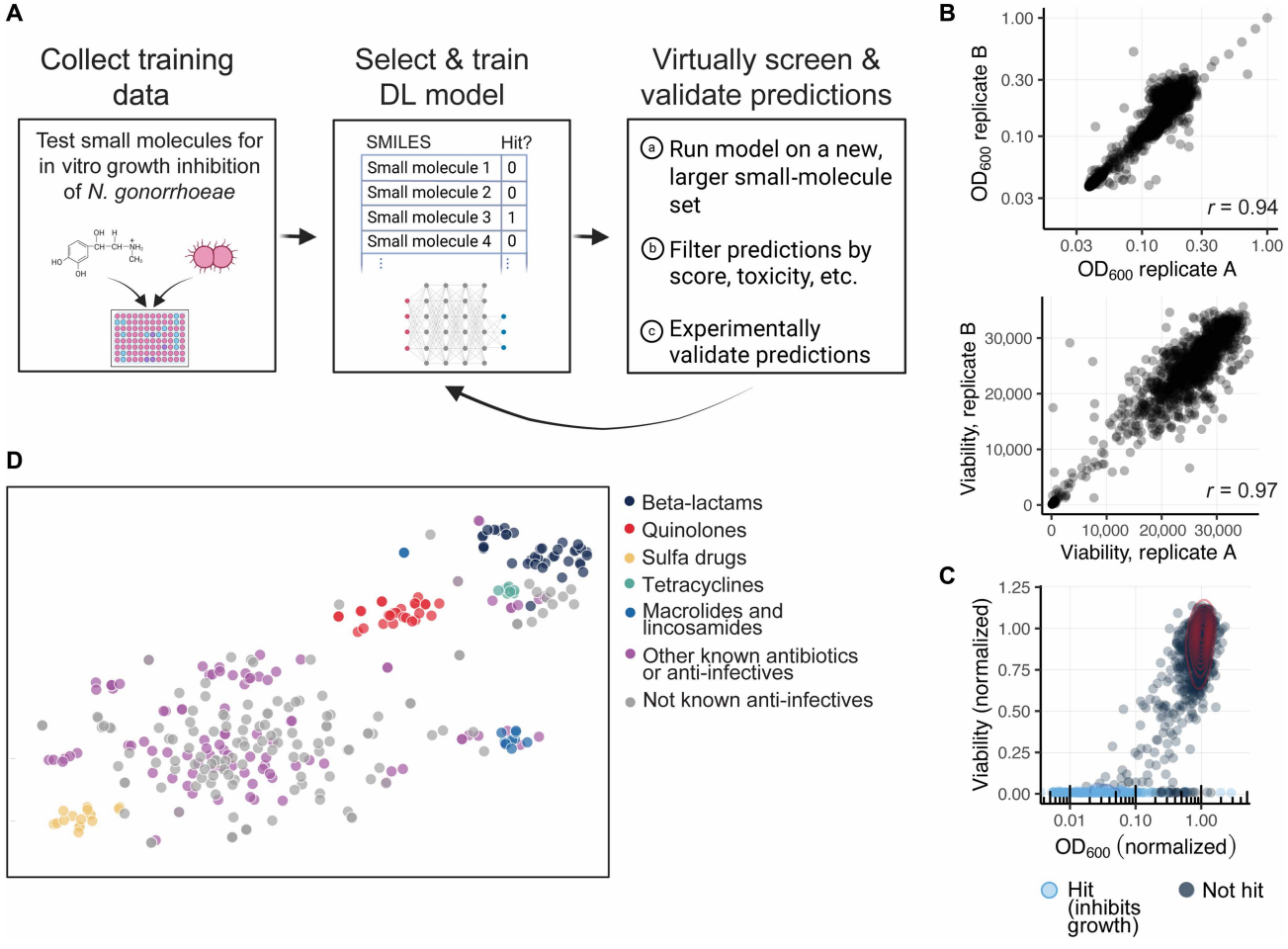

Fig. 1. HTS of small molecules for *N. gonorrhoeae* growth inhibitory activity reveals non–anti-infective drugs with antibacterial activity. (**A**) Schematic of the DL-based antibiotic discovery approach. (**B**) *N. gonorrhoeae* ATCC 49226 growth (OD_{600}; top) and viability (resazurin-based dye; bottom) readouts from the Pharmakon-1.7K screen at a 50-μM final concentration ($n = 1755$). The Pearson correlation coefficient (r) among replicates is shown. (**C**) Annotation of growth inhibitory hit molecules (blue, $n = 340$) and nonhits (gray, $n = 1415$). Contours of a two-dimensional density estimate are shown in red. **(D)** A *t*-distributed stochastic neighbor embedding (*t*-SNE) mapping of chemical space of the 340 Pharmakon-1.7K hits, annotated by known antibiotic class.

We then evaluated the hyperparameter-optimized models by holding out test data from the models with two different methods: random split and scaffold split. Scaffold-split test sets are a more difficult test of model generalizability because they contain compounds with Murcko scaffolds that were not found in the training set (*17*). Performance on scaffold-split data is especially important in discovery efforts where the aim is to find antibacterial scaffolds. We found that D-MPNNs had the highest performance for both types of test sets, as measured by the AUPRC and AUROC (Fig. 2D and Materials and Methods).

To assess performance of the D-MPNN under budget and time constraints that restrict testing to a fixed number of N compounds, we simulated in vitro validation of the N highest-scoring compounds in the test set. For each N, we evaluated the precision (hit rate) and recall (capture rate, or the fraction of all hits found) for the D-MPNN. The D-MPNN exhibited high precision (80%) and recall (31.5%) for the top $N = 100$ compounds (Fig. 2E). Similar precision and recall values (~50%) were found after sampling the top $N = 250$ compounds. In addition, given the cost of training data acquisition and the overwhelming majority of negative (nonhit) data points, we asked whether including such a large amount of negative training data was beneficial to model performance and what type of negative data maximized performance. D-MPNN performance consistently improved with larger training sets, even when the additional data points were all negative (nonhits) (fig. S2). Randomly selected negative training data performed as well as or better than diverse negative data or negative data that were structurally similar to hits (fig. S2). These analyses suggest that D-MPNNs can effectively prioritize compounds in large libraries for screens of antigonococcal activity.

D-MPNNs accurately enrich for antigonococcal compounds from chemical libraries with sensitivity to structural divergence from training compounds

To determine how well the D-MPNN model performs on structurally distinct small molecules, we used the Broad Institute's internal library of 799,147 compounds ("Broad-800K") to design three prospective evaluation sets of increasing difficulty and desirability (evaluation sets 1, 2, and 3) and compared them with a random selection of 30 compounds (Fig. 3A). We selected compounds from the Broad-800K for empirical testing on the basis of their antigonococcal

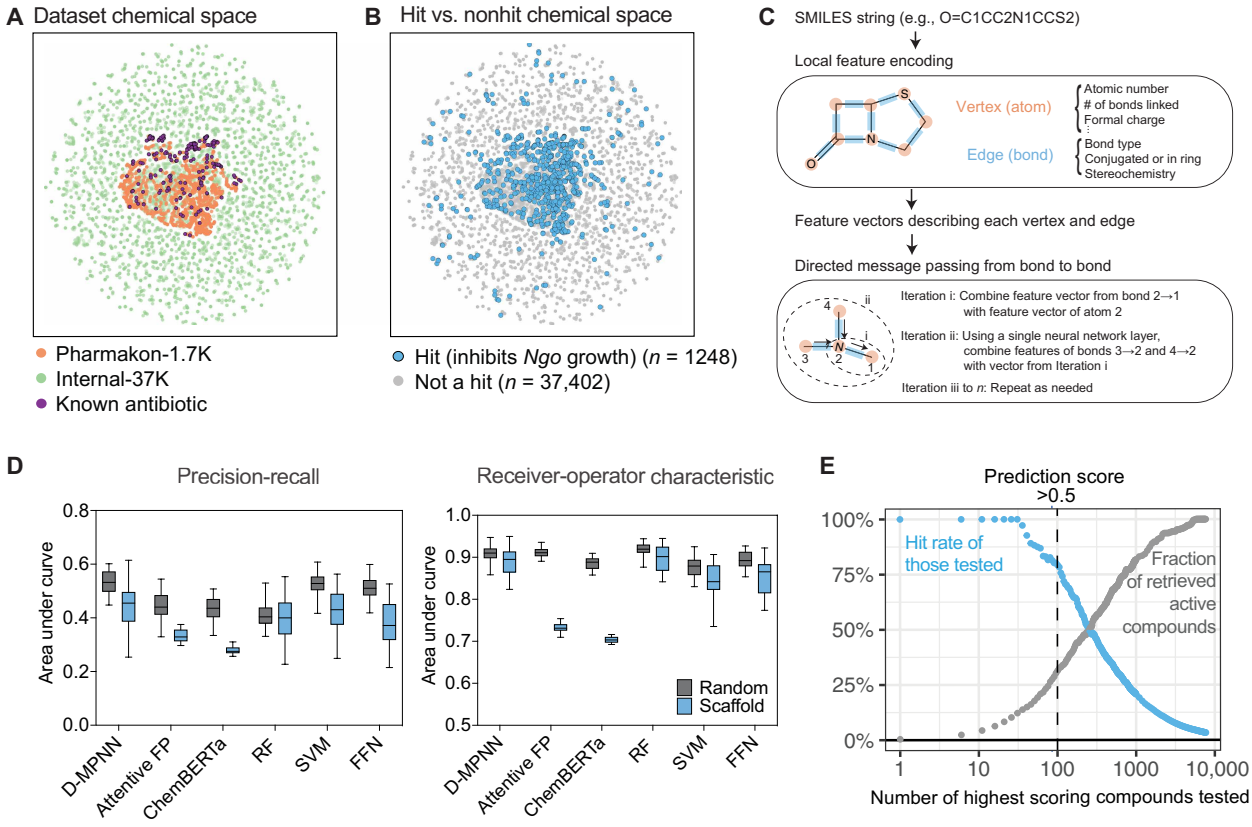

Fig. 2. Training dataset expansion and selection of a DL model for predicting *N. gonorrhoeae* (*Ngo*) growth inhibition. (**A**) *t*-SNE mapping of the Pharmakon-1.7K (orange, $n = 1755$), Internal-37K (green, $n = 36{,}895$), and known antibiotics (purple, $n = 566$). (**B**) Annotation of the active hits (blue, $n = 1248$) and inactive compounds (gray, $n = 37{,}402$) on the same *t*-SNE mapping as (A). (**C**) Schematic for the message passing through bonds that occurs in a D-MPNN. (**D**) Comparison of six models, trained on the Pharmakon-1.7K and Internal-37K libraries and evaluated using random-split (gray) or scaffold-split (blue) cross-validation folds. $N = 20$ folds for ChemBERTa and Attentive FP; $N = 30$ folds for RF, SVM, FFN, and D-MPNN models. Boxes indicate 25th to 75th percentiles; whiskers show min/max values. (**E**) Simulation of real-world screening using a D-MPNN trained and hyperparameter optimized on 80% of the combined Pharmakon-1.7K and Internal-37K training sets and tested on the class-balanced 20% held-out test set. The hit rate of those tested (precision; blue) and the fraction of retrieved active compounds in the test set (recall; gray) are shown as a function of the *N* highest scoring compounds tested. The dashed line ($N = 100$) indicates a prediction score threshold of 0.5 for antigonococcal activity.

model prediction score (Fig. 3B) and criteria that they be structurally distinct from each other (fig. S3), from known antibiotics (Fig. 3C), and from compounds in the training set (Fig. 3D). Tanimoto similarity (Tan Sim) on chemical fingerprints was used to quantify structural similarity (range: 0 to 1, where 1 = identical). Evaluation sets 2 and 3 contained more desirable compounds than set 1 for two reasons. The first is that they were more structurally distinct from known antibiotics, which we expect to be more difficult for the model to predict because it requires more generalization (Fig. 3E). The second is that they were predicted not to be cytotoxic to human liver and primary skeletal muscle cells using previously described DL cytotoxicity models (*12*).

Eighty-six percent (44 of 51) of compounds in evaluation set 1 inhibited *N. gonorrhoeae* ATCC 49226 growth at 100 μM (Fig. 3F and table S4). Several of these compounds were recently described in the literature as antimicrobials, such as aurothiomalate and marinopyrrole (*24*, *25*), providing further confidence in the model predictions. The DL model predictions were largely correct even in the more challenging evaluation sets, with 54 and 50% hit rates in sets 2 and 3, respectively, at 100 μM. Most compounds in the Broad-800K library are not known to be antibacterial, and none of 30 randomly selected compounds inhibited ATCC 49226 growth at concentrations at or below 100 μM. These data highlight the ability of a DL model to find rare compounds with antibacterial activity that are structurally dissimilar from training examples.

Prospective virtual screening of 5 million commercially available compounds identifies antigonococcal hits, with enrichment for nitro-heterocyclic scaffolds

Given the encouraging validation rates of the D-MPNN model and to sample a larger chemical space, we then deployed the model on a ~5.3 million compound library assembled from three commercial vendors ("Commercial-5M"). Fifty-eight compounds remained after stringent filtering for high D-MPNN model scores (prediction score > 0.9), low similarity to known antibiotics and the training set hits, no pan-assay interference compounds (PAINS) (*26*) and ≤2 Brenk alerts (*27*), low lipophilicity, and diversity (Fig. 4A). Of these 58 compounds, 22 (38%) inhibited growth of the wild-type ATCC 49226 strain when tested at 50 μM or lower (Fig. 4A and table S5).

Nitro (-NO_2) functional groups were found in 63% (14 of 22) of the in vitro validated hits from the Commercial-5M library and 40% (27 of 67) from evaluation sets. Further minimum inhibitory

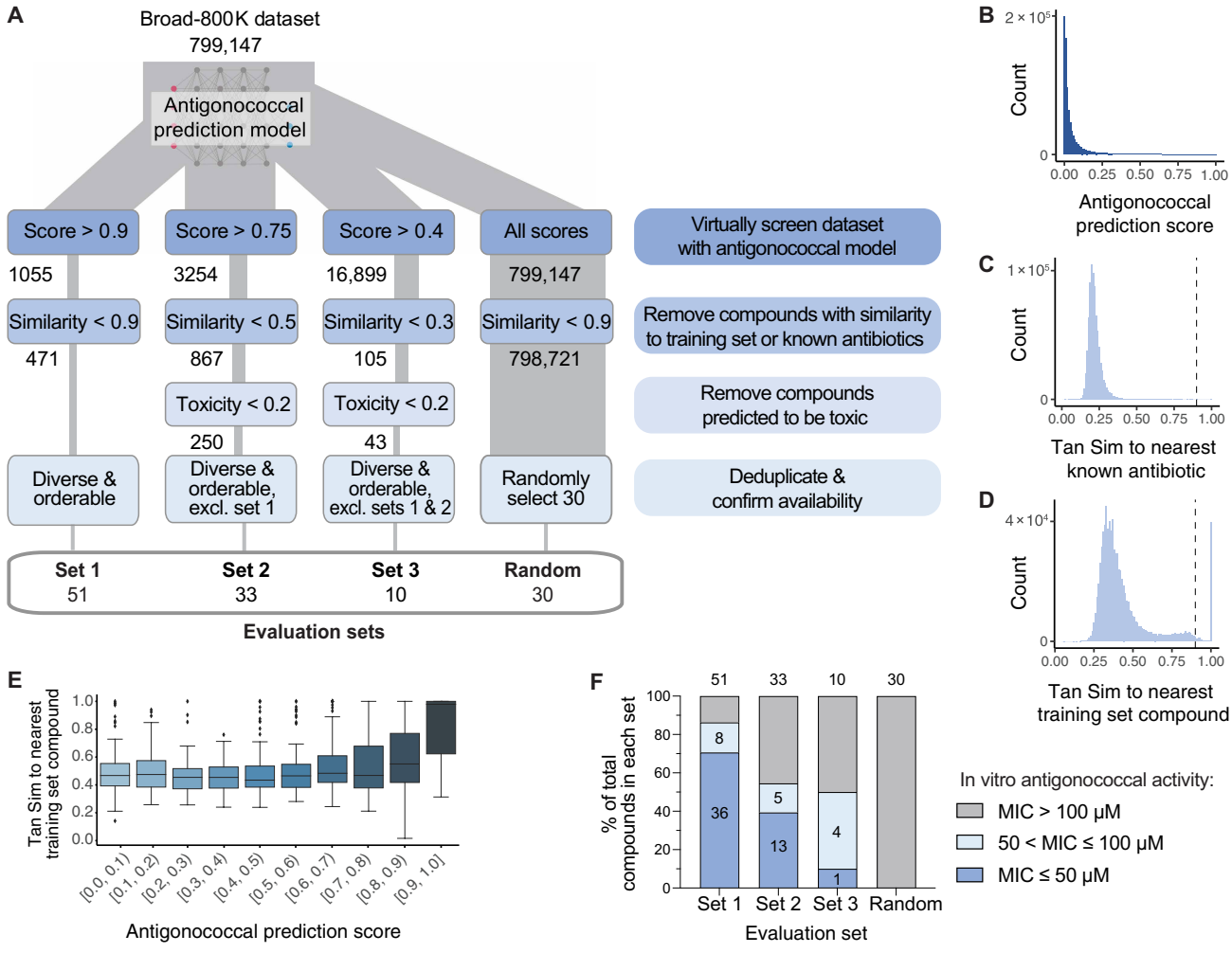

Fig. 3. Testing D-MPNN model performance on evaluation sets derived from the Broad-800K library with varying tiers of difficulty. (**A**) Schematic of the filtering steps of the Broad-800K library (n = 799,147) used to generate evaluation sets 1 to 3 and the random baseline comparator set, where model score was not considered. After a virtual screen of the Broad-800K library, candidates were filtered for structural distinctness by Tan Sim to known antibiotics and the training set; set 3 represented the most structurally distinct compounds. Compounds predicted to have human cytotoxicity were removed from sets 2 and 3. Selection for in vitro testing was determined by deduplication, subsampling for structural diversity, compound availability, and purity. (**B**) Distribution of antigonococcal model prediction scores for all Broad-800K compounds. (**C**) Distribution of Broad-800K compounds with respect to the Tan Sim to the nearest known antibiotic. The dashed line represents the first threshold (0.9) used for filtering. (**D**) Distribution of Broad-800K compounds with respect to the nearest training set hit compound. Dashed line represents the first threshold (0.9) used for filtering. (**E**) Relationship between model prediction scores and the Tan Sim to the nearest training set compound. Model prediction scores for all Broad-800K compounds were binned, and 100 molecules were randomly sampled from each binned interval, without replacement, for a total of 1000 molecules represented in the box plot. Boxes extend from the 25th to 75th percentiles, and whiskers represent minimum and maximum values. (**F**) Distribution of in vitro MICs of the compounds in each evaluation set against *N. gonorrhoeae* ATCC 49226.

concentration (MIC) testing revealed that some nitro-containing compounds were extremely potent with MICs of 0.04 to 0.06 μg/ml in ATCC 49226 (fig. S4A). Nitro groups are found in commonly prescribed antibiotics such as nitrofurantoin and metronidazole as well as the recently FDA-approved antituberculosis drug called pretomanid (*28*), which are all prodrugs that require reductive activation in the bacterial cell by nitroreductases (*29*, *30*). To understand the DL model's predilection for nitro-containing compounds, we determined the substructures in the nitro-containing compounds that had high model-predicted antibiotic activity on their own, also known as "rationales" (fig. S4B) (*12*). By incorporating the experimental MIC data of the 31 compounds grouped by the four rationales, SAR analysis revealed that the potency of nitrofuran compounds was inversely correlated with the presence of a carboxamide group (e.g., 5-nitrofuran-2-carboxamide) (fig. S4B). Nitrothiazoles and nitrothiophenes were also uniformly potent against the wild-type strain. Further testing of the most potent and structurally distinct nitro-containing compounds (fig. S4C) revealed MICs that were 8 to 64 times higher in three multidrug-resistant (MDR) *N. gonorrhoeae* strains compared with the wild-type, which reduced the initially promising selectivity indices (fig. S4D). Although substructures of these compounds may still have interesting antibacterial properties, we chose to exclude nitro-containing compounds from further analysis because of their reduced efficacy in MDR strains and perceived liabilities of toxicity and mutagenicity.

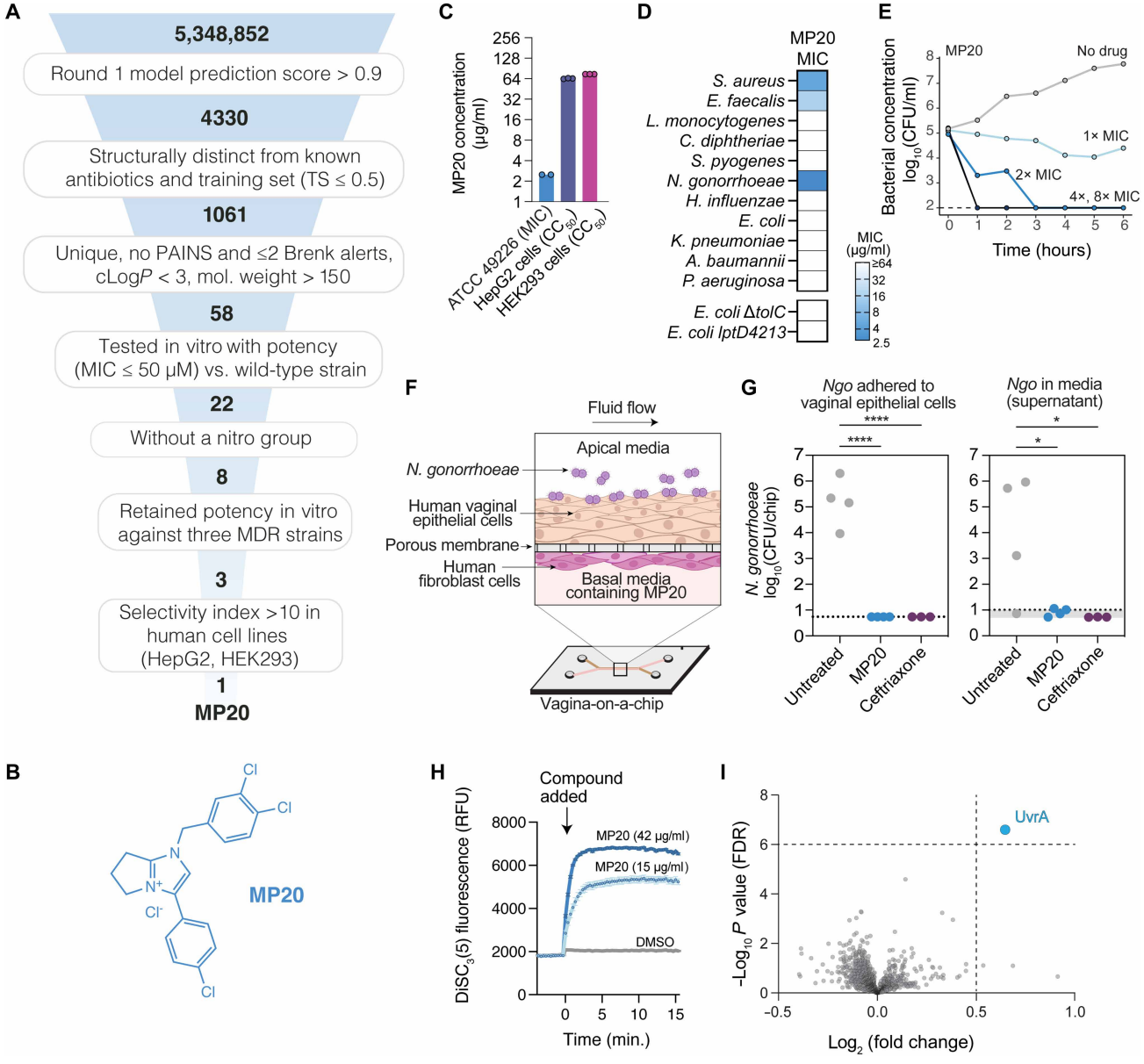

Fig. 4. Discovery of an inhibitor of *N. gonorrhoeae* growth through DL-guided screening of a commercial 5.3 million compound library. (**A**) Multistep filtering to identify promising antigonococcal compounds by screening the Commercial-5M library with the D-MPNN model. (**B**) Structure of MP20, a pyrrolo[1,2-a]imidazole-containing compound, identified from the Commercial-5M dataset (model score of 0.944). (**C**) Comparison of the MP20 MIC (blue) with the CC_{50} values for two human cell lines: HepG2 (purple) and HEK293 (pink). Points represent biological replicates, and bars indicate mean values. (**D**) Heatmap of MICs of MP20 against a variety of Gram-positive and Gram-negative organisms. Results represent two biological replicates. (**E**) Time-kill kinetics of *N. gonorrhoeae* ATCC 49226 cells treated with MP20 at 1× to 8× agar MIC or a no-drug control. (**F**) Schematic for the in vitro human vagina-on-a-chip setup, where a microfluidic device made of an optically transparent polymer enables a three-dimensional culture system with fluid flow. Not illustrated is the Zoë Culture Module that provided dynamic culture conditions. (**G**) MP20 bacterial CFU per chip in the adhered and nonadhered fractions after 48 hours of basal treatment with MP20 ($n = 4$), ceftriaxone ($n = 3$), or an untreated control ($n = 4$). Dotted line represents the limit of detection (LoD) of CFU plating, with slight variability because of chip-to-chip variability in recovered volume. Statistical significance determined by one-way ANOVA with Dunnett's multiple comparisons testing relative to untreated. *$P < 0.05$; ****$P \leq 0.0001$. (**H**) $DiSC_3(5)$ fluorescence of *N. gonorrhoeae* ATCC 49226 cells treated with MP20 at two concentrations or DMSO. Mean and SD of two biological replicates. (**I**) Volcano plot of proteomic profiling of *N. gonorrhoeae* after 20 min of MP20 treatment, showing the most significantly up-regulated protein, UvrA. RFU, relative fluorescence units. FDR, false discovery rate.

Compound MP20 exhibits activity against Gram-positive organisms and MDR *N. gonorrhoeae* with rapid bactericidal kinetics and low frequency of spontaneous resistance

Of the eight remaining active compounds without nitro groups (Fig. 4A), it was notable that two compounds (MP20 and MP21, fig. S5A) were analogs with model prediction scores of >0.9 that contained pyrrolo[1,2-a]imidazole groups and were structurally dissimilar from known antibiotics and training set compounds (fig. S5, B and C). We next tested the eight compounds to determine whether they retained potency against three MDR *N. gonorrhoeae* strains

with an MIC of ≤16 μg/ml, which is a commonly used threshold of activity for a promising hit compound in the early discovery stage. For the three compounds that retained potency, we then assessed for human cytotoxicity by determining the half-maximal cytotoxic concentration (CC_{50}) in a hepatoma G2 (HepG2) human liver carcinoma cell line and a human embryonic kidney 293T (HEK293) cell line to calculate the compound's selectivity index (SI; SI = CC_{50}/MIC in wild-type strain). An SI of >10 is considered acceptable in early-stage discovery (*9*). Of these, only one compound remained, MP20 (Fig. 4B), which had SIs of 25 and 30 in HepG2 and HEK293 cells, respectively (Fig. 4C). MP20 maintained efficacy against several antibiotic-resistant strains, including one that was recently found in the US to be nonsusceptible or resistant to all recommended first- and second-line antibiotics [*N. gonorrhoeae* AR Bank (ARB) no. 1281; Table 1]. MP20 contains an imidazole, which is reported to have antibacterial activity (*31*), but our SAR studies and those reported in the literature confirmed that the imidazole ring and even MP20's Murcko scaffold (*32*), which lacks three chlorine substituents, do not independently inhibit bacterial growth (table S6). This indicated that MP20 is a candidate hit for further characterization.

We next sought to further characterize the antibacterial activity of MP20. MP20 inhibited the growth of both methicillin-susceptible and methicillin-resistant strains of *Staphylococcus aureus* but was not efficacious against any Gram-negative bacteria tested other than *N. gonorrhoeae* (Fig. 4D). We then tested 39 additional *N. gonorrhoeae* isolates, which were highly enriched for strains with resistance to standard-of-care antibiotics (table S7). We found that MP20 MIC values were significantly associated with the outer membrane channel porin PorB type ($P = 0.0045$ by multivariable linear regression) but not with other known antimicrobial resistance genes, including the *mtrR* promoter that regulates efflux pump expression (fig. S5D). Specifically, MDR strains with mutations in PorB1b at positions 120 and 121—which are known to decrease permeation of penicillin, ceftriaxone, and tetracycline (*33*)—had elevated MP20 MICs of up to 16 μg/ml (fig. S5E).

In time-kill experiments with ATCC 49226, MP20 had rapid, concentration-dependent bactericidal effects, with >3-log killing in 1 hour at 4× agar MIC (Fig. 4E), which was faster than ceftriaxone (fig. S5F). To estimate the rate at which clinical resistance could emerge, we determined the frequency of spontaneous resistance. After 72 hours of incubation, no resistant colonies emerged on any

Table 1. Antibacterial activity of clinically used antibiotics and DL-identified compounds MP20 and A1. Current and previous first-line antibiotics of ceftriaxone (CTX), ciprofloxacin (CIP), azithromycin (AZM), and tetracycline (TET) are listed for reference. WT, wild type; AMR, antimicrobial resistance; S91F, Ser^{91}→Phe; A39T, Ala^{39}→Thr; G120K, Gly^{120}→Lys; A121D, Ala^{121}→Asp; A121S, Ala^{121}→Ser; A121N, Ala^{121}→Asn; A121G, Ala^{121}→Gly.

Strain	Relevant strain characteristics					Minimum inhibitory concentration (μg/ml)					
	penA	*gyrA*	*mtrCDE* efflux pump	*porB* outer membrane permeability	Horizontally acquired AMR genes	CTX	CIP	AZM	TET	MP20	A1
ATCC 49226	XXII NonMosaic	WT	*mtrR* A39T	WT	None	0.008	0.004	0.25	0.5	2.5	2
ATCC 700825 (FA1090)	I NonMosaic	WT	WT	WT	None	0.001	0.004	0.0625	0.031	2.5	1
ARB no. 1281	60.001 Mosaic	S91F	Increased expression	Decreased, G120K, A121D	bla_{TEM}	1	16	2	2	8	4
ARB no. 0175	II NonMosaic	WT	Resistance-associated *mtrD* allele	WT	None	0.008	0.015	16	1	8	4
ARB no. 0179	II NonMosaic	WT	Resistance-associated *mtrD* allele	WT	None	0.008	0.015	8	1	8	4
ARB no. 0181	II NonMosaic	WT	Resistance-associated *mtrD* allele	Decreased, A121S	None	0.03	0.015	256	2	8	4
ARB no. 0166	XXXIV Mosaic	S91F	Increased expression	Decreased, G120K, A121N	None	0.125	8	1	4	10	4
ARB no. 0187	XXXIV Mosaic	S91F	Resistance-associated promoter, *mtrC*, and *mtrD* alleles	WT	None	0.03	4	2	1	8	4
GCGS0759	XXXIV Mosaic	S91F	Increased expression	Decreased, G120K, A121N	None	0.063	16	8	2	8	2
HHH023	XIX NonMosaic	S91F	Increased expression	Decreased, G120K, A121G	bla_{TEM}, *tetM*	0.015	16	0.125	>64	8	4

of the plates containing MP20 at 2×, 4×, or 8× agar MIC, indicating a low frequency of spontaneous resistance less than 8.3×10^{-9}.

MP20 shows antibacterial activity in a microfluidic vagina-on-a-chip model of gonococcal infection

Given that MP20 had an attractive profile as a hit compound, we next sought to test its antibacterial efficacy in a tissue-mimicking microenvironment. The microfluidic vagina-on-a-chip (Vagina Chip) was an appealing model for candidate testing because of the use of primary human cells (vaginal epithelial and uterine fibroblast cells grown on opposite sides of a porous membrane), unique recapitulation of the three-dimensional vaginal environment with tissue-tissue and tissue-fluid interfaces, and simulation of distinct fluid flows with a continuous stratified epithelium that prevents mixing of the apical and basal media on the basal and apical sides (Fig. 4F). The Vagina Chip was recently used to study human vaginal microbial-host interactions under microaerophilic conditions (*34*, *35*), and, here, we adapted those conditions to support *N. gonorrhoeae*. Before commencing the Vagina Chip experiments, we ensured that *N. gonorrhoeae* was not cytotoxic to epithelial cells at the relevant pathogen load used in all drug studies (fig. S6A). We also confirmed that MP20 was stable in the basal and apical media used in the Vagina Chip (fig. S6, B to D), maintained its MIC in medium with 10% fetal calf serum (fig. S6E), and was not toxic to the vaginal epithelial and uterine fibroblast cells at the concentrations tested (fig. S6F).

To model the outcome of systemic compound administration in vaginal gonorrhea infection, Vagina Chips were inoculated with *N. gonorrhoeae* ATCC 49226 in the apical channel, the bacteria were allowed to adhere to the vaginal epithelial cells for 2 hours, and MP20 or ceftriaxone was then added to the basal channel. Bacteria-only control chips did not receive any antibiotic. After 2 days of incubation at 37°C and 5% CO_2 under continuous basal flow and intermittent apical flow, culture was performed to quantify both free-floating *N. gonorrhoeae* and *N. gonorrhoeae* adhered to or invaded into the vaginal epithelial cells. Both MP20 and ceftriaxone resulted in undetectable levels of both adhered and nonadhered *N. gonorrhoeae*, whereas the no-drug controls had a mean adhered bacterial load of 1.56×10^5 colony-forming units (CFUs) per chip and unadhered load of 8.22×10^3 CFU per chip (Fig. 4G). The reductions in *N. gonorrhoeae* load were significant in both the adhered [$P < 0.0001$, one-way analysis of variance (ANOVA) with Dunnett's multiple comparisons testing of both MP20 and ceftriaxone versus the untreated control] and unadhered fractions ($P = 0.0309$ by one-way ANOVA; $P = 0.0374$ of MP20 versus untreated and $P = 0.0403$ of ceftriaxone versus untreated with Dunnett's multiple comparisons testing). These results support that MP20 can cross human cell barriers and retains antibacterial activity without overt human cell toxicity in this complex organ-like microenvironment.

MP20 induces rapid membrane depolarization and oxidative stress

We further investigated the mechanism by which MP20 was killing *N. gonorrhoeae* using chemical, proteomic, and genetic approaches. We found that MP20 induced rapid, dose-dependent membrane depolarization and dequenching of the voltage-sensitive (3,3′)-dipropylthiadicarbocyanine iodide [$DiSC_3(5)$] dye (Fig. 4H) (*36*) but had no effect on the fluidity of the bacterial membrane (fig. S7A). To understand how MP20 induces rapid membrane depolarization, we sought to evolve resistant mutants by performing serial passaging of two MDR *N. gonorrhoeae* strains in sub-MIC concentrations of MP20. The MIC of strain ARB no. 0199 did not change after 11 passages in Graver Wade medium (fig. S7B), whereas the MIC of strain ARB no. 0175 only slightly increased from 4 to 6 μg/ml after eight passages (fig. S7C). We performed subsequent passages in either Graver Wade alone or supplemented with 0.01% Tween (for mild permeabilization) or 0.2 M sorbitol (for hypertonicity) to stress the bacterial membrane and hasten the mutational process (*37*). However, the MIC only slightly increased to 8 μg/ml, and strains passaged under all three conditions appeared to suffer a fitness cost with failure to grow after the fourteenth passage.

To more deliberately search for protein targets of MP20, we applied the Protein Integral Solubility Alteration (PISA) coupled to mass spectrometry assay. PISA identifies protein targets of small molecules by assessing compound-induced changes in protein thermal stability by exposing cells or cellular lysates to a temperature gradient after ligand treatment (*38*). However, MP20 did not produce any specific protein "hits"—no single protein's thermostability was significantly affected by MP20 treatment ($P > 0.05$)—suggesting that MP20 either does not strongly or directly bind to protein targets detectable under our experimental conditions.

To explore the system-level effects of MP20, we used the 2′,7′-dichlorodihydrofluorescein diacetate (H2DCFDA) assay, a widely used fluorogenic probe for monitoring intracellular reactive oxygen species (ROS). Upon passive diffusion into cells, H2DCFDA is deacetylated by intracellular esterases to a nonfluorescent intermediate, which is subsequently oxidized by ROS into the highly fluorescent 2′,7′-dichlorofluorescein. Thus, increasing fluorescence intensity provides a quantitative measure of ROS accumulation and oxidative stress. *N. gonorrhoeae* ATCC 49226 cells exposed to MP20 at 10× MIC displayed a time-dependent increase in fluorescence, consistent with elevated ROS production (fig. S7D). This apparent oxidative stress signature prompted us to perform proteomic expression profiling to assess downstream cellular responses. Early after MP20 exposure, we observed an increase in the DNA damage recognition protein UvrA (ultraviolet repair protein A), a component of the UvrABC nucleotide excision repair complex (Fig. 4I), whose activation is often associated with DNA lesion detection and repair initiation (*39*). After four serial passages under MP20 exposure at half MIC, we observed up-regulation of recombination protein N (RecN), a protein central to homologous recombination repair of double-strand breaks, suggesting potential genotoxic stress (fig. S7E). Together, these data suggest that MP20 elicits a multifaceted stress response in *N. gonorrhoeae*, including membrane depolarization, oxidative stress, induction of nucleotide excision repair, and activation of homologous recombination pathways, which resembles the cellular responses triggered by known bactericidal antibiotics (*40*, *41*).

Model retraining leads to the discovery of A1, which narrowly yet comprehensively targets *N. gonorrhoeae*

To further enrich for distinct compounds, we used an active learning approach to rescreen the Broad-800K library. We first retrained the D-MPNN model using an expanded training set that included the binarized growth inhibition data from the evaluation sets ($n = 94$) and Commercial-5M set ($n = 58$). We then used the retrained model in conjunction with additional filters that removed compounds containing nitro groups and sulfonamides and required a less stringent retrained model prediction score (>0.5) and lipophilicity criteria (cLog$P < 5$) and a more stringent threshold for

structural liabilities (≤1 Brenk alert) (Fig. 5A). Chemical uniqueness was determined by low similarity to known antibiotics and the training set hits (Tan Sim ≤ 0.7) and no known antibacterial activity reported in the literature. Of the 61 compounds that passed these filters and could be tested, 11 had an MIC of ≤50 μM against *N. gonorrhoeae* ATCC 49226, for an 18% hit rate, and six of those retained potency against three MDR strains. Of those, three compounds were nontoxic to HepG2 and HEK293 cell lines at 100 μM. A literature search revealed that two of these three compounds had human receptor targets and thus were at risk of off-target activity in vivo. The final remaining compound, named A1 (Fig. 5B), had SIs of 47 and 58 in HepG2 and HEK293 cells, respectively (Fig. 5C), did not have reported human receptor targets, had no PAINS or Brenk alerts, and was selected for further testing. A1 contains an aminothiazole (*42*), but the mere presence of an aminothiazole group in a compound was not sufficient to confer antigonococcal activity in our SAR studies (table S8).

Further characterization of compound A1 revealed that it was narrow in spectrum, with activity only against *N. gonorrhoeae* among the human pathogenic bacterial species tested (Fig. 5D). When tested against a panel of 49 wild-type and MDR *N. gonorrhoeae* strains, including ARB no. 1281 (Table 1 and table S7), the population-level A1 MIC_{50} was 2 μg/ml and MIC_{90} was 4 μg/ml (Fig. 5E). Compound A1 was bactericidal, exhibiting 4-log killing in 4 hours at 4× MIC, which was slower than MP20 but faster than ceftriaxone (Fig. 5F and fig. S4F). The frequency of spontaneous resistance in three *N. gonorrhoeae* strains was very low: $\leq 5 \times 10^{-9}$ at 8× agar MIC (Fig. 5G).

The MICs of A1 were not affected by the two major *N. gonorrhoeae* resistance mechanisms that affect structurally diverse compounds: decreased porin-dependent permeability because of *porB* mutations and increased expression or activity of the *mtrCDE* efflux pump, which confers resistance to multiple antimicrobials and also effluxes dyes, hormones, and detergents (Table 1, table S7, and Fig. 5E) (*43*, *44*). To probe whether membrane permeability limits A1 activity, we conducted a checkerboard assay combining A1 with polymyxin B, a membrane-disrupting agent (*45*), and observed synergy between the two compounds (fig. S8A). These results are consistent with the hypothesis that, owing to its lipophilic nature, A1 may cross the cell membrane via self-permeation to reach its target.

Proteomic analyses demonstrate alanine racemase as the protein target of A1

We next sought to determine the mechanism by which A1 kills *N. gonorrhoeae*. Unlike MP20, A1 did not cause a notable change in

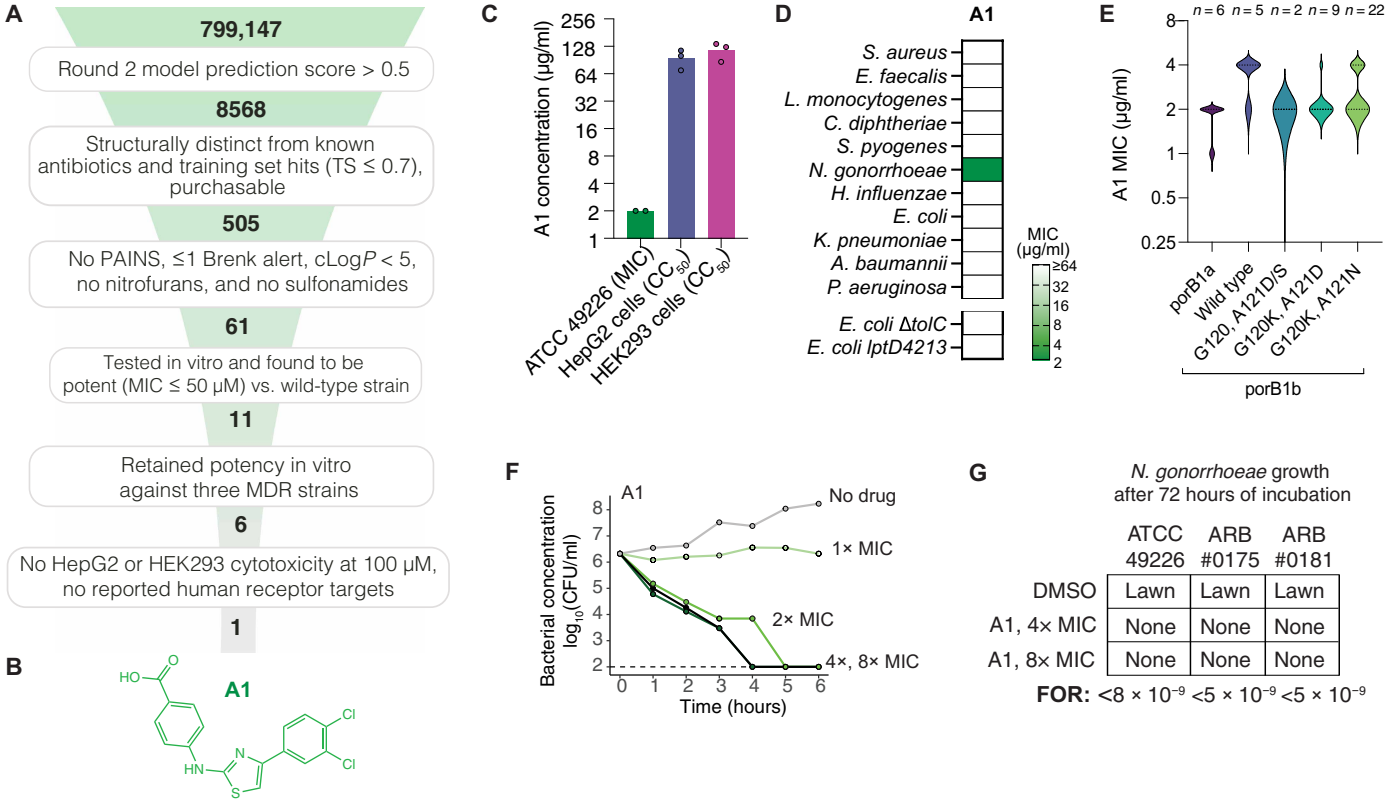

Fig. 5. Discovery of a second inhibitor of *N. gonorrhoeae* growth through DL-guided screening of the Broad-800K library. (**A**) Multistep filtering process to identify promising antigonococcal compounds by rescreening the Broad-800K library with the retrained, round 2 D-MPNN DL model. (**B**) Structure of compound A1, an aminothiazole-containing compound discovered from the Broad-800K dataset (model score of 0.52). (**C**) Comparison of the A1 MIC (green) with the CC_{50} values for two human cell lines: HepG2 (purple) and HEK293 (pink). Points represent biological replicates, and bars indicate mean values. (**D**) Heatmap of MICs of A1 against a variety of Gram-positive and Gram-negative organisms, demonstrating their narrow spectrum of activity. Results represent two biological replicates. (**E**) MICs of A1 against a panel of 49 *N. gonorrhoeae* isolates, classified by their PorB1a/PorB1b type. (**F**) Time-kill kinetics of *N. gonorrhoeae* ATCC 49226 cells treated with A1 at 1× to 8× agar MIC or a no-drug control. (**G**) Determination of the frequency of resistance for A1 in ATCC 49226, ARB no. 0175, and ARB no. 0181 when tested at 4× or 8× agar MIC or a no-drug control. Results represent two biological replicates. DMSO, dimethyl sulfoxide.

the membrane potential as measured by the $DiSC_3(5)$ dye (fig. S8B) but did show a membrane rigidifying effect in the Laurdan fluorescence assay (Fig. 6A). To better understand the mechanism underlying this observation, we performed PISA on lysates of *N. gonorrhoeae*, which revealed alanine racemase (Alr) as a distinct target ($P < 0.0005$ and arbitrary cutoff of $\log_2$ fold change ≥ 0.5) (Fig. 6, B and C). Alr is a critical enzyme that catalyzes the interconversion of L-alanine and D-alanine, an essential precursor in peptidoglycan biosynthesis (*46*).

We also found that A1 has activity against the model Gram-positive bacterium *Bacillus subtilis*, which encodes a homologous Alr involved in peptidoglycan biosynthesis (fig. S9, A to D). Thus, we tested Alr as the functional target of A1 using a *B. subtilis* strain with constitutive expression of a single guide RNA (sgRNA)–targeting *alrA* ($sgRNA^{alrA}$) and inducible *dcas9* expression driven by a xylose-inducible promoter (*47*). Treatment of the *B. subtilis* $sgRNA^{alrA}$ strain with 0.05% xylose reduced *alrA* gene expression to 5% of basal levels, whereas xylose treatment had no effect on the *alrA* expression level in a control *B. subtilis* strain that did not express an sgRNA (fig. S8C). Knockdown of *alrA*-sensitized cells to A1 treatment at one-quarter MIC (Fig. 6D) showed a significant decrease in growth relative to control ($P = 0.025$, unpaired two-tailed *t* test; fig. S9E), suggesting that reduced Alr abundance increases susceptibility to A1.

Last, to obtain direct molecular evidence that A1 binds Alr, we heterologously expressed and purified recombinant *N. gonorrhoeae* Alr (fig. S10) and then used nuclear magnetic resonance (NMR) spectroscopy to assess target engagement. Reference one-dimensional ^{1}H and ^{13}C NMR spectra of A1 were recorded providing the chemical shift fingerprint of the molecule, with assignments established using two-dimensional correlation spectroscopy (COSY), heteronuclear single-quantum coherence (HSQC), and heteronuclear multiple-bond correlation (HMBC) experiments (Fig. 6E and fig. S11). To test for direct interaction, we performed a saturation transfer difference (STD) NMR experiment, selectively saturating the protein while monitoring the ligand signals and focused on the aromatic region of the spectrum (6 to 8 parts per million), where A1 displays isolated signals from its aromatic functional groups. A1 showed a distinct STD signal in the spectrum compared with the control, indicating efficient magnetization transfer from the protein to the ligand (Fig. 6F). This occurs only when the ligand is in close proximity to the protein to allow for efficient magnetization transfer, thus strongly indicating direct binding. Overall, our integrative approach confirms that A1 engages Alr as its protein target.

A1 decreases *N. gonorrhoeae* titers in a topical mouse vaginal infection model

Last, we sought to test A1's antibacterial activity in vivo. Compound A1 was well tolerated in BALB/c mice, with a maximum tolerated dose of 100 mg/kg (the highest dose tested) when given once a day systemically via an intraperitoneal injection and at least 50 mg/kg when given every 6 hours intraperitoneally (200 mg/kg per day). The compound's half-life was >145 min in human liver microsomes and 70.3 min in mouse liver microsomes, indicating good metabolic stability (table S9). The plasma protein binding fraction was high, at 99.9% in both human and mouse plasma (table S10).

We next performed in vivo testing in a mouse vaginal model of *N. gonorrhoeae* infection (Fig. 6G). The mice were inoculated intravaginally with ATCC 49226 and treated intravaginally at five times in the 24 hours postinfection. Two hours after the last dose, the animals were euthanized, and vaginal lavages were performed for quantitative titering. As expected, ceftriaxone treatment resulted in undetectable levels of *N. gonorrhoeae*, whereas the vehicle control had a median *N. gonorrhoeae* load of 2.0×10^5 CFU/ml (Fig. 6H). Compound A1 significantly reduced the median bacterial load by two logs relative to vehicle ($P = 0.0223$, Fig. 6H). Thus, these data support the activity of compound A1 in complex in vivo settings. We anticipate that further medicinal chemistry optimization, focusing on quantifying and increasing free drug concentrations (*48*) and improving potency and selectivity, will generate analogs with attractive pharmacokinetic and pharmacodynamic properties.

DISCUSSION

This work demonstrates that DL-based virtual screening can efficiently identify antigonococcal small-molecule hits, which promises to address the high and unmet clinical need for new antimicrobials. Here, we have shown that these compounds can retain potency against even the most highly resistant strains of *N. gonorrhoeae*, exhibit selective killing toward bacteria, and act through orthogonal mechanisms from those of existing first-line antibiotics. When trained on a large and diverse set of 38,650 compounds that we tested against an *N. gonorrhoeae* strain, DL models enabled time and cost-efficient screening with in vitro validation rates as high as 70% in the Broad-800K library, as compared with a baseline rate of 2.5% in the training set. We used this screening approach to uncover two compounds, a pyrroloimidazole and an aminothiazole, without previously described antigonococcal activity. Mechanistic studies revealed that the candidate MP20 disrupts the bacterial membrane and induces DNA damage upon both immediate exposure and prolonged passage. The second compound, A1, demonstrated superior activity by targeting the enzyme Alr, which is required for bacterial cell wall biosynthesis. We also demonstrate that these compounds can reduce bacterial loads in a human dynamic in vitro organ model and a mouse in vivo model, respectively.

Through comprehensive validation, we identify three important considerations when implementing a DL model for antimicrobial discovery. First, DL-guided antimicrobial discovery is fundamentally a generalization task, aiming to identify molecules that are structurally distinct from known antimicrobials, which often comprise most training set hits. Generalizability is improved by obtaining a structurally diverse training set and choosing an appropriate model architecture. The D-MPNN used here exhibited the highest AUPRC values on random- and scaffold-split data among the models that we tested. Although the attention-based GNNs and chemical LLM also performed well on random splits, the D-MPNN demonstrated particular resilience against the performance drops typically associated with scaffold-based evaluation, indicating better ability to generalize. Second, selecting appropriate model prediction score thresholds for virtual screening has important downstream implications, with trade-offs between yield and novelty. Compounds with the highest prediction scores tend to be most structurally similar to training set hits, whereas explicit downstream filtering for structural dissimilarity to training set compounds (including known antibiotics) biases predictions toward structural novelty at the cost of lower validation rates. Third, augmenting DL model predictions with additional filtering steps is often needed. The models developed here focus on predicting gonococcal growth inhibition, and using a phenotypic label has the advantage of potentially identifying compounds that

act through growth inhibitory mechanisms distinct from those of known antibiotics. However, toxicity remains an important consideration for phenotypic screening, and additional filtering steps are needed, in part, to remove indiscriminately toxic compounds. Here, we accomplished this by removing compounds with structural liabilities and counterscreening for cytotoxicity in human cell lines. Together, these considerations will better inform future work in DL-guided antimicrobial discovery.

MP20 and A1 appear to act via different mechanisms. MP20 likely acts, at least in part, by perturbing the bacterial membrane, which may subsequently promote ROS accumulation, oxidative stress, and downstream activation of DNA repair pathways. This could represent

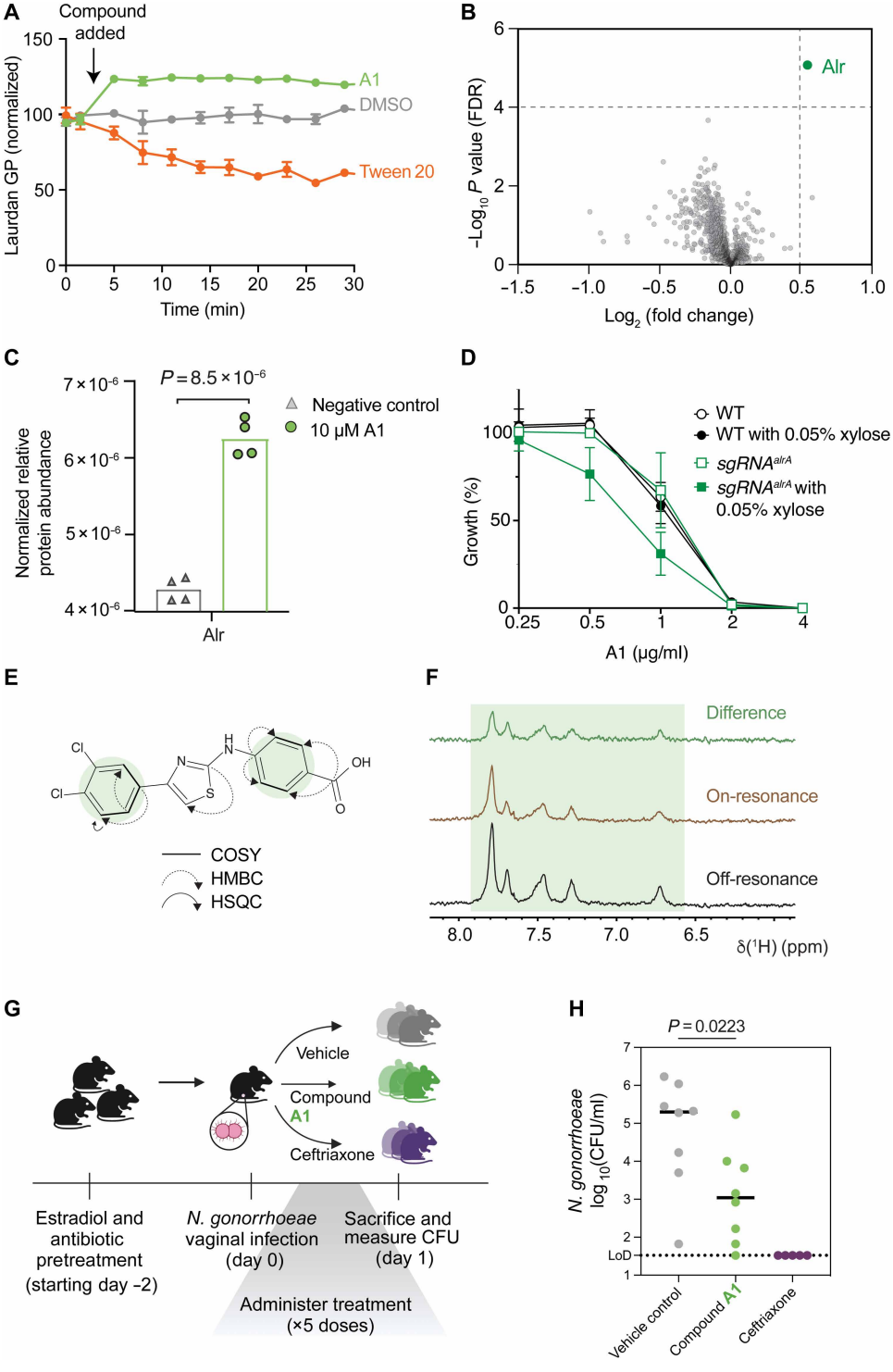

Fig. 6. Mechanism of action and in vivo studies for compound A1. (**A**) Assessment of membrane fluidity by measuring Laurdan generalized polarization (GP) of ATCC 49226 treated with A1, DMSO (negative control), or Tween 20 (positive control). Mean and SD of two biological replicates are shown. (**B**) Volcano plot for PISA experiment performed on A1-treated *N. gonorrhoeae* lysates, identifying Alr as markedly stabilized. (**C**) Quantification of Alr normalized relative protein abundances from PISA, performed on A1- or DMSO-treated *N. gonorrhoeae* lysates. Statistical significance determined with a two-sided *t* test. (**D**) Effect of CRISPRi-mediated knockdown of *alrA* on *B. subtilis* growth in the presence of A1. Growth of a strain with constitutive expression of a sgRNA^{alrA} was compared with that of a wild-type strain without sgRNA expression. Xylose (0.05%) was used for *dcas9* induction. Mean and SD of four biological replicates are shown. WT, wild type. (**E**) Structural assignment of A1 based on proton and carbon correlations from COSY, HMBC, and HSQC NMR experiments. (**F**) STD NMR spectra of A1 with recombinant Alr. ppm, parts per million. (**G**) Schematic of the in vivo study of compound A1 in the *N. gonorrhoeae* vaginal infection model using ATCC 49226. (**H**) *N. gonorrhoeae* titers in vaginal lavage fluid. Dotted line represents the LoD. Horizontal lines indicate the median. Experimental treatments consisted of vehicle control ($n = 8$), A1 ($n = 8$), or ceftriaxone ($n = 5$). Significance determined by one-way ANOVA with Dunnett's multiple comparisons relative to vehicle.

an indirect route to genotoxic stress, consistent with the observed up-regulation of UvrA and RecN. In contrast, our data suggest that A1 engages Alr, a clinically underexplored enzyme target (*49*). Further studies will be required to define the details of drug-target engagement. A1 may act as a competitive inhibitor or potentially as an allosteric modulator, given that Alr has been reported to form higher-order assemblies. Structural characterization of A1-Alr interactions may identify pharmacophores and atomic contacts underlying A1's activity, thereby providing a foundation for hit optimization through quantitative SAR modeling.

Our study has several limitations. Although our training set is more than an order of magnitude larger than previous datasets for *N. gonorrhoeae* (*18*, *50*), model prediction accuracy would likely benefit from increased data acquisition over larger, more diverse chemical spaces (*51*). We also recognize limitations in the D-MPNN model architecture, such as its focus on two-dimensional rather than three-dimensional chemical structure. Emerging DL models may outperform our current model in identifying antibiotic candidates. Although our model can virtually screen ultralarge, make-on-demand libraries, we focused here on in-stock compounds for cost and time efficiency. We did not exhaustively screen the chemical landscape, did not focus on traditional Gram-negative physiochemical properties (*52*), and may have inadvertently filtered out promising compounds. Additional cross-pathogen characterization would more definitively establish the compounds' spectrum of activity. Last, when envisioning the translational potential of compounds identified by our model, similar to the vast majority of hits found through traditional screening campaigns, additional optimization is needed to achieve in vivo efficacy when delivered systemically (*53*).

Overall, we have described the development, validation, and deployment of a DL-guided approach to *N. gonorrhoeae* antimicrobial discovery. We have introduced a publicly available set of 38,650 compounds tested for growth inhibition of *N. gonorrhoeae*, which we hope will be used to train and benchmark additional DL models. By prioritizing species-specific activity rather than broad cell inhibition, our approach provides an opportunity to find previously unidentified antimicrobial targets, such as those found specifically in the *Neisseria* cell membranes, providing a distinct path for future antimicrobial development. The combination of computational and experimental screening techniques offers a promising avenue for the high-throughput discovery of antibacterials active against *N. gonorrhoeae*.

MATERIALS AND METHODS

Study design

The objective of this study was to develop and validate a DL model to predict antigonococcal activity from chemical structures and then deploy the model to discover existing small molecules with previously unrecognized activity. We collected a training set of 38,650 molecules, including almost all known antigonococcal small molecules. We compared a variety of model architectures trained on these data and found that the D-MPNN model had the best performance. After optimizing the D-MPNN model, we used it to screen three evaluation sets from the Broad-800K library, a set of 5,348,852 commercially available compounds, and the entire Broad-800K library. We identified two molecules, called MP20 and A1, which had selectivity indices of >10 and retained activity against MDR *N. gonorrhoeae* strains. We further characterized their antibacterial properties and mechanisms of action and then tested the compounds using two vaginal gonococcal infection models, with MP20 tested in a Vagina Chip model and A1 in a mouse model. In the mouse model, we randomly assigned cages to treatment conditions but were not blinded. Experiments were performed in at least biological duplicates, unless otherwise noted.

Statistical analysis

All statistical analyses were performed using GraphPad Prism (version 10.6.1) or RStudio (version 2024.12.0+467). Individual data points are provided in data file S1. Details of the statistical tests used, the exact value and meaning of *n*, as well as the meaning of the error bars are provided in the figure legends. The individual statistical test used (e.g., Student's *t* test and one-way ANOVA) was based on the data type and experimental design. Animal sample sizes were determined by power calculations in GraphPad Prism to detect a 1- to 2-log fold change in effect size and mouse availability. Group allocation was determined by cage, where each cage contained three to five mice that all received the same randomly assigned treatment. No data were excluded from the study analyses. Strain GCGS0759 was obtained from the CDC; requests for this strain should be directed to CDC. Strain HHH023 was provided to Y.H.G. under a material transfer agreement with the Division of Microbiology and Infectious Diseases, National Institute of Allergy and Infectious Diseases.

Supplementary Materials

The PDF file includes:
Materials and Methods
Figs. S1 to S12
Tables S1 to S10
Legend for data file S1
References (*56*–*80*)

Other Supplementary Material for this manuscript includes the following:
Data file S1
MDAR Reproducibility Checklist

REFERENCES AND NOTES

1. Centers for Disease Control and Prevention, "Antibiotic resistant threats in the United States, 2019" (US Department of Health and Human Services, CDC, 2019).
2. J. F. Elias, M. U. Vogel, in *Manual of Clinical Microbiology*, K. C. Carroll, M. A. Pfaller, M. L. Landry, A. J. McAdam, R. Patel, S. S. Richter, D. W. Warnock, Eds. (ASM Press, 2019), pp. 641–642.
3. M. Unemo, M. M. Lahra, M. Escher, S. Eremin, M. J. Cole, P. Galarza, F. Ndowa, I. Martin, J. R. Dillon, M. Galas, P. Ramon-Pardo, H. Weinstock, T. Wi, WHO global antimicrobial resistance surveillance for *Neisseria gonorrhoeae* 2017-18: A retrospective observational study. *Lancet Microbe* **2**, e627–e636 (2021).
4. V. Ouk, C. D. Pham, T. Wi, S. J. van Hal, M. M. Lahra, EGASP Cambodia working group, The enhanced gonococcal surveillance programme, Cambodia. *Lancet Infect. Dis.* **23**, e332–e333 (2023).
5. J. L. Reimche, C. D. Pham, S. J. Joseph, S. Hutton, J. C. Cartee, Y. Ruan, M. Breaux, C. Ivanof, A. Joshi, M. DeMartino, J. E. Kirby, L. A. Barbee, E. N. Kersh, K. A. Roosevelt, K. K. Hsu, Novel strain of multidrug non-susceptible *Neisseria gonorrhoeae* in the USA. *Lancet Infect. Dis.* **24**, e149–e151 (2024).
6. B. D. Bax, P. F. Chan, D. S. Eggleston, A. Fosberry, D. R. Gentry, F. Gorrec, I. Giordano, M. M. Hann, A. Hennessy, M. Hibbs, J. Huang, E. Jones, J. Jones, K. K. Brown, C. J. Lewis, E. W. May, M. R. Saunders, O. Singh, C. E. Spitzfaden, C. Shen, A. Shillings, A. J. Theobald, A. Wohlkonig, N. D. Pearson, M. N. Gwynn, Type IIA topoisomerase inhibition by a new class of antibacterial agents. *Nature* **466**, 935–940 (2010).
7. A. A. Miller, G. L. Bundy, J. E. Mott, J. E. Skepner, T. P. Boyle, D. W. Harris, A. E. Hromockyj, K. R. Marotti, G. E. Zurenko, J. B. Munzner, M. T. Sweeney, G. F. Bammert, J. C. Hamel, C. W. Ford, W. Z. Zhong, D. R. Graber, G. E. Martin, F. Han, L. A. Dolak, E. P. Seest, J. C. Ruble, G. M. Kamilar, J. R. Palmer, L. S. Banitt, A. R. Hurd, M. R. Barbachyn, Discovery and characterization of QPT-1, the progenitor of a new class of bacterial topoisomerase inhibitors. *Antimicrob. Agents Chemother.* **52**, 2806–2812 (2008).

8. L. Yao, T. Tian, D. Zou, X. Lu, N. Jiang, X. Feng, T. Zheng, Z. Tang, Y. Lin, Z. Ning, J. Jiang, M. Ye, P. Zhou, Stepwise evolution and clonal enrichment of gepotidacin resistance in *Neisseria gonorrhoeae*. *Antimicrob. Agents Chemother.* **70**, e0170625 (2026).
9. D. J. Payne, M. N. Gwynn, D. J. Holmes, D. L. Pompliano, Drugs for bad bugs: Confronting the challenges of antibacterial discovery. *Nat. Rev. Drug Discov.* **6**, 29–40 (2007).
10. O. O. Grygorenko, D. S. Radchenko, I. Dziuba, A. Chuprina, K. E. Gubina, Y. S. Moroz, Generating multibillion chemical space of readily accessible screening compounds. *iScience* **23**, 101681 (2020).
11. J. M. Stokes, K. Yang, K. Swanson, W. Jin, A. Cubillos-Ruiz, N. M. Donghia, C. R. MacNair, S. French, L. A. Carfrae, Z. Bloom-Ackermann, V. M. Tran, A. Chiappino-Pepe, A. H. Badran, I. W. Andrews, E. J. Chory, G. M. Church, E. D. Brown, T. S. Jaakkola, R. Barzilay, J. J. Collins, A deep learning approach to antibiotic discovery. *Cell* **180**, 688–702.e13 (2020).
12. F. Wong, E. J. Zheng, J. A. Valeri, N. M. Donghia, M. N. Anahtar, S. Omori, A. Li, A. Cubillos-Ruiz, A. Krishnan, W. Jin, A. L. Manson, J. Friedrichs, R. Helbig, B. Hajian, D. K. Fiejtek, F. F. Wagner, H. H. Soutter, A. M. Earl, J. M. Stokes, L. D. Renner, J. J. Collins, Discovery of a structural class of antibiotics with explainable deep learning. *Nature* **626**, 177–185 (2024).
13. G. Liu, D. B. Catacutan, K. Rathod, K. Swanson, W. Jin, J. C. Mohammed, A. Chiappino-Pepe, S. A. Syed, M. Fragis, K. Rachwalski, J. Magolan, M. G. Surette, B. K. Coombes, T. Jaakkola, R. Barzilay, J. J. Collins, J. M. Stokes, Deep learning-guided discovery of an antibiotic targeting *Acinetobacter baumannii*. *Nat. Chem. Biol.* **19**, 1342–1350 (2023).
14. D. Rogers, M. Hahn, Extended-connectivity fingerprints. *J. Chem. Inf. Model.* **50**, 742–754 (2010).
15. S. Chithrananda, G. Grand, B. Ramsundar, ChemBERTa: Large-scale self-supervised pretraining for molecular property prediction. arXiv:2010.09885 [cs.LG] (2020).
16. E. J. Zheng, J. A. Valeri, I. W. Andrews, A. Krishnan, P. Bandyopadhyay, M. N. Anahtar, A. Herneisen, F. Schulte, B. Linnehan, F. Wong, J. M. Stokes, L. D. Renner, S. Lourido, J. J. Collins, Discovery of antibiotics that selectively kill metabolically dormant bacteria. *Cell Chem. Biol.* **31**, 712–728.e9 (2024).
17. K. Yang, K. Swanson, W. Jin, C. Coley, P. Eiden, H. Gao, A. Guzman-Perez, T. Hopper, B. Kelley, M. Mathea, A. Palmer, V. Settels, T. Jaakkola, K. Jensen, R. Barzilay, Analyzing learned molecular representations for property prediction. *J. Chem. Inf. Model.* **59**, 3370–3388 (2019).
18. S. Foerster, T. N. Gustafsson, A. R. Brochado, V. Desilvestro, A. Typas, M. Unemo, The first wide-scale drug repurposing screen using the Prestwick Chemical Library (1200 bioactive molecules) against *Neisseria gonorrhoeae* identifies high in vitro activity of auranofin and many additional drugs. *APMIS* **128**, 242–250 (2020).
19. T. M. Oeschger, D. C. Erickson, Visible colorimetric growth indicators of *Neisseria gonorrhoeae* for low-cost diagnostic applications. *PLOS ONE* **16**, e0252961 (2021).
20. M. Noto Guillen, C. Li, B. Rosener, A. Mitchell, Antibacterial activity of nonantibiotics is orthogonal to standard antibiotics. *Science* **384**, 93–100 (2024).
21. Z. Xiong, D. Wang, X. Liu, F. Zhong, X. Wan, X. Li, Z. Li, X. Luo, K. Chen, H. Jiang, M. Zheng, Pushing the boundaries of molecular representation for drug discovery with the graph attention mechanism. *J. Med. Chem.* **63**, 8749–8760 (2020).
22. K. Huang, T. Fu, W. Gao, Y. Zhao, Y. Roohani, J. Leskovec, C. W. Coley, C. Xiao, J. Sun, M. Zitnik, Therapeutics Data Commons: Machine learning datasets and tasks for drug discovery and development. arXiv:2102.09548 [cs.LG] (2021).
23. W. Ahmad, E. Simon, S. Chithrananda, G. Grand, B. Ramsundar, ChemBERTa-2: Towards chemical foundation models. arXiv:2209.01712 [cs.LG] (2022).
24. A. Elkashif, M. N. Seleem, Investigation of auranofin and gold-containing analogues antibacterial activity against multidrug-resistant *Neisseria gonorrhoeae*. *Sci. Rep.* **10**, 5602 (2020).
25. N. M. Haste, C. C. Hughes, D. N. Tran, W. Fenical, P. R. Jensen, V. Nizet, M. E. Hensler, Pharmacological properties of the marine natural product marinopyrrole A against methicillin-resistant *Staphylococcus aureus*. *Antimicrob. Agents Chemother.* **55**, 3305–3312 (2011).
26. J. Baell, M. A. Walters, Chemistry: Chemical con artists foil drug discovery. *Nature* **513**, 481–483 (2014).
27. R. Brenk, A. Schipani, D. James, A. Krasowski, I. H. Gilbert, J. Frearson, P. G. Wyatt, Lessons learnt from assembling screening libraries for drug discovery for neglected diseases. *ChemMedChem* **3**, 435–444 (2008).
28. K. Nepali, H. Y. Lee, J. P. Liou, Nitro-group-containing drugs. *J. Med. Chem.* **62**, 2851–2893 (2019).
29. C. C. McOsker, P. M. Fitzpatrick, Nitrofurantoin: Mechanism of action and implications for resistance development in common uropathogens. *J. Antimicrob. Chemother.* **33** (suppl. A), 23–30 (1994).
30. I. E. Eke, R. B. Abramovitch, Functions of nitroreductases in mycobacterial physiology and drug susceptibility. *J. Bacteriol.* **207**, e0032624 (2025).
31. N. Rani, A. Sharma, R. Singh, Imidazoles as promising scaffolds for antibacterial activity: A review. *Mini Rev. Med. Chem.* **13**, 1812–1835 (2013).
32. S. Demchenko, R. Lesyk, O. Yadlovskyi, J. Zuegg, A. G. Elliott, I. Drapak, Y. Fedchenkova, Z. Suvorova, A. Demchenko, Synthesis, antibacterial and antifungal activity of new 3-aryl-5*H*-pyrrolo[1,2-*a*]imidazole and 5*H*-Imidazo[1,2-*a*]azepine quaternary salts. *Molecules* **26**, 4253 (2021).
33. M. Unemo, W. M. Shafer, Antimicrobial resistance in *Neisseria gonorrhoeae* in the 21st century: Past, evolution, and future. *Clin. Microbiol. Rev.* **27**, 587–613 (2014).
34. A. Gulati, A. Jorgenson, A. Junaid, D. E. Ingber, Modeling healthy and dysbiotic vaginal microenvironments in a human vagina-on-a-chip. *J. Vis. Exp.* **204**, e66486 (2024).
35. G. Mahajan, E. Doherty, T. To, A. Sutherland, J. Grant, A. Junaid, A. Gulati, N. LoGrande, Z. Izadifar, S. S. Timilsina, V. Horvath, R. Plebani, M. France, I. Hood-Pishchany, S. Rakoff-Nahoum, D. S. Kwon, G. Goyal, R. Prantil-Baun, J. Ravel, D. E. Ingber, Vaginal microbiome-host interactions modeled in a human vagina-on-a-chip. *Microbiome* **10**, 201 (2022).
36. J. D. Te Winkel, D. A. Gray, K. H. Seistrup, L. W. Hamoen, H. Strahl, Analysis of antimicrobial-triggered membrane depolarization using voltage sensitive dyes. *Front. Cell Dev. Biol.* **4**, 29 (2016).
37. M. T. Doyle, J. R. Jimah, T. Dowdy, S. I. Ohlemacher, M. Larion, J. E. Hinshaw, H. D. Bernstein, Cryo-EM structures reveal multiple stages of bacterial outer membrane protein folding. *Cell* **185**, 1143–1156.e13 (2022).
38. M. Gaetani, P. Sabatier, A. A. Saei, C. M. Beusch, Z. Yang, S. L. Lundstrom, R. A. Zubarev, Proteome integral solubility alteration: A high-throughput proteomics assay for target deconvolution. *J. Proteome Res.* **18**, 4027–4037 (2019).
39. K. J. Wozniak, L. A. Simmons, Bacterial DNA excision repair pathways. *Nat. Rev. Microbiol.* **20**, 465–477 (2022).
40. M. A. Kohanski, D. J. Dwyer, B. Hayete, C. A. Lawrence, J. J. Collins, A common mechanism of cellular death induced by bactericidal antibiotics. *Cell* **130**, 797–810 (2007).
41. D. J. Dwyer, P. A. Belenky, J. H. Yang, I. C. MacDonald, J. D. Martell, N. Takahashi, C. T. Chan, M. A. Lobritz, D. Braff, E. G. Schwarz, J. D. Ye, M. Pati, M. Vercruysse, P. S. Ralifo, K. R. Allison, A. S. Khalil, A. Y. Ting, G. C. Walker, J. J. Collins, Antibiotics induce redox-related physiological alterations as part of their lethality. *Proc. Natl. Acad. Sci. U.S.A.* **111**, E2100–E2109 (2014).
42. T. Sato, K. Yamawaki, Cefiderocol: Discovery, chemistry, and in vivo profiles of a novel siderophore cephalosporin. *Clin. Infect. Dis.* **69**, S538–S543 (2019).
43. K. E. Hagman, W. Pan, B. G. Spratt, J. T. Balthazar, R. C. Judd, W. M. Shafer, Resistance of *Neisseria gonorrhoeae* to antimicrobial hydrophobic agents is modulated by the mtrRCDE efflux system. *Microbiology* **141** (pt. 3), 611–622 (1995).
44. M. Olesky, S. Zhao, R. L. Rosenberg, R. A. Nicholas, Porin-mediated antibiotic resistance in *Neisseria gonorrhoeae*: Ion, solute, and antibiotic permeation through PIB proteins with penB mutations. *J. Bacteriol.* **188**, 2300–2308 (2006).
45. S. Manioglu, S. M. Modaresi, N. Ritzmann, J. Thoma, S. A. Overall, A. Harms, G. Upert, A. Luther, A. B. Barnes, D. Obrecht, D. J. Muller, S. Hiller, Antibiotic polymyxin arranges lipopolysaccharide into crystalline structures to solidify the bacterial membrane. *Nat. Commun.* **13**, 6195 (2022).
46. N. A. Thornberry, H. G. Bull, D. Taub, K. E. Wilson, G. Gimenez-Gallego, A. Rosegay, D. D. Soderman, A. A. Patchett, Mechanism-based inactivation of alanine racemase by 3-halovinylglycines. *J. Biol. Chem.* **266**, 21657–21665 (1991).
47. J. M. Peters, A. Colavin, H. Shi, T. L. Czarny, M. H. Larson, S. Wong, J. S. Hawkins, C. H. S. Lu, B. M. Koo, E. Marta, A. L. Shiver, E. H. Whitehead, J. S. Weissman, E. D. Brown, L. S. Qi, K. C. Huang, C. A. Gross, A comprehensive, CRISPR-based functional analysis of essential genes in bacteria. *Cell* **165**, 1493–1506 (2016).
48. D. A. Smith, L. Di, E. H. Kerns, The effect of plasma protein binding on in vivo efficacy: Misconceptions in drug discovery. *Nat. Rev. Drug Discov.* **9**, 929–939 (2010).
49. K. G. Anthony, U. Strych, K. R. Yeung, C. S. Shoen, O. Perez, K. L. Krause, M. H. Cynamon, P. A. Aristoff, R. A. Koski, New classes of alanine racemase inhibitors identified by high-throughput screening show antimicrobial activity against *Mycobacterium tuberculosis*. *PLOS ONE* **6**, e20374 (2011).
50. J. C. Pereira, S. S. Daher, K. M. Zorn, M. Sherwood, R. Russo, A. L. Perryman, X. Wang, M. J. Freundlich, S. Ekins, J. S. Freundlich, Machine learning platform to discover novel growth inhibitors of *Neisseria gonorrhoeae*. *Pharm. Res.* **37**, 141 (2020).
51. G. Scalia, S. T. Rutherford, Z. Lu, K. R. Buchholz, N. Skelton, K. Chuang, N. Diamant, J.-C. Hutter, J. M. Luescher, A. Miu, J. Blaney, L. Gendelev, E. Skippington, G. Zynda, N. Dickson, M. Koziarski, Y. Bengio, A. Regev, M. W. Tan, T. Biancalani, Deep-learning-based virtual screening of antibacterial compounds. *Nat. Biotechnol.* 10.1038/s41587-025-02814-6 (2025).
52. R. O'Shea, H. E. Moser, Physicochemical properties of antibacterial compounds: Implications for drug discovery. *J. Med. Chem.* **51**, 2871–2878 (2008).
53. World Health Organization, *Target Product Profile for Therapy of Diagnosed Uncomplicated Gonorrhoea* (World Health Organization, 2020).
54. jackievaleri, jackievaleri/ngonorrhoeae_abx_ml_discovery: v1.1, version 1.1, Zenodo (2026); https://doi.org/10.5281/zenodo.19902261.
55. J. A. Valeri, Models and data for NG-ML, version 2, Zenodo (2026); https://doi.org/10.5281/zenodo.19899206.
56. Centers for Disease Control and Prevention, "CDC & FDA Antimicrobial Resistance Isolate Bank"; https://wwwn.cdc.gov/ARIsolateBank/.

57. H. Liu, E. Vidyaprakash, M. W. Schmerer, D. C. Pham, S. St Cyr, E. N. Kersh, A culture collection of 50 *Neisseria gonorrhoeae* isolates. *Microbiol. Resour. Announc.* **9**, e00699-20 (2020).
58. Y. H. Grad, S. R. Harris, R. D. Kirkcaldy, A. G. Green, D. S. Marks, S. D. Bentley, D. Trees, M. Lipsitch, Genomic epidemiology of gonococcal resistance to extended-spectrum cephalosporins, macrolides, and fluoroquinolones in the United States, 2000-2013. *J. Infect. Dis.* **214**, 1579–1587 (2016).
59. C. C. Bristow, T. D. Mortimer, S. Morris, Y. H. Grad, O. O. Soge, E. Wakatake, R. Pascual, S. M. Murphy, K. E. Fryling, P. C. Adamson, J. A. Dillon, N. R. Parmar, H. H. L. Le, H. Van Le, R. M. Ovalles Urena, N. Mitchev, K. Mlisana, T. Wi, S. P. Dickson, J. D. Klausner, Whole-genome sequencing to predict antimicrobial susceptibility profiles in *Neisseria gonorrhoeae*. *J. Infect. Dis.* **227**, 917–925 (2023).
60. J. J. Wade, M. A. Graver, A fully defined, clear and protein-free liquid medium permitting dense growth of *Neisseria gonorrhoeae* from very low inocula. *FEMS Microbiol. Lett.* **273**, 35–37 (2007).
61. F. Pedregosa, G. Varoquaux, A. Gramfort, V. Michel, B. Thirion, O. Grisel, M. Blondel, A. Müller, J. Nothman, G. Louppe, P. Prettenhofer, R. Weiss, V. Dubourg, J. Vanderplas, A. Passos, D. Cournapeau, M. Brucher, M. Perrot, É. Duchesnay, Scikit-learn: Machine learning in python. *J. Mach. Learn. Res.* **12**, 2825–2830 (2011).
62. J. Bergstra, R. Bardenet, Y. Bengio, B. Kégl, Algorithms for hyper-parameter optimization. *Adv. Neural Inf. Proces. Syst.* **24**, 2546–2554 (2011).
63. T. Wolf, L. Debut, V. Sanh, J. Chaumond, C. Delangue, A. Moi, P. Cistac, T. Rault, R. Louf, M. Funtowicz, J. Davison, S. Shleifer, P. von Platen, C. Ma, Y. Jernite, J. Plu, C. Xu, T. Le Scao, S. Gugger, M. Drame, Q. Lhoest, A. Rush, "Transformers: State-of-the-art natural language processing" in *Proceedings of the 2020 Conference on Empirical Methods in Natural Language Processing: System Demonstrations* (Association for Computational Linguistics, 2020), pp. 38–45.
64. Z. Wu, B. Ramsundar, E. N. Feinberg, J. Gomes, C. Geniesse, A. S. Pappu, K. Leswing, V. Pande, MoleculeNet: A benchmark for molecular machine learning. *Chem. Sci.* **9**, 513–530 (2018).
65. Q. Guo, S. Hernandez-Hernandez, P. J. Ballester, Scaffold splits overestimate virtual screening performance. arXiv:2406.00873 [q-bio.QM] (2024).
66. M. Ashton, J. M. Barnard, F. Casset, M. H. Charlton, G. M. Downs, D. Gorse, J. D. Holliday, R. Lahana, P. Willett, Identification of diverse database subsets using property-based and fragment-based molecular descriptions. *Quant. Struct. Act. Relat.* **21**, 598–604 (2002).
67. J. Hert, J. J. Irwin, C. Laggner, M. J. Keiser, B. K. Shoichet, Quantifying biogenic bias in screening libraries. *Nat. Chem. Biol.* **5**, 479–483 (2009).
68. A. Krishnan, M. N. Anahtar, J. A. Valeri, W. Jin, N. M. Donghia, L. Sieben, A. Luttens, Y. Zhang, S. M. Modaresi, A. Hennes, J. Fromer, P. Bandyopadhyay, J. C. Chen, D. Rehman, R. Desai, P. Edwards, R. S. Lach, M. S. Aschtgen, M. Gaborieau, M. Gaetani, S. G. Palace, S. Omori, L. Khonde, Y. S. Moroz, B. Blough, C. Jin, E. Loh, Y. H. Grad, A. A. Saei, C. W. Coley, F. Wong, J. J. Collins, A generative deep learning approach to de novo antibiotic design. *Cell* **188**, 5962–5979.e22 (2025).
69. Clinical and Laboratory Standards Institute, *Performance Standards for Antimicrobial Susceptibility Testing* (Clinical and Laboratory Standards Institute, ed. 30, CLSI supplement M100, 2020).
70. Clinical and Laboratory Standards Institute, *Methods for Dilution Antimicrobial Susceptibility Tests for Bacteria that Grow Aerobically* (Clinical and Laboratory Standards Institute, ed. 11, CLSI standard M07, 2018).
71. S. Foerster, M. Unemo, L. J. Hathaway, N. Low, C. L. Althaus, Time-kill curve analysis and pharmacodynamic modelling for in vitro evaluation of antimicrobials against *Neisseria gonorrhoeae*. *BMC Microbiol.* **16**, 216 (2016).
72. S. M. Modaresi, R. Sugiyama, N. D. T. Tram, R. P. Jakob, C.-S. Phan, A. A. Saei, Y. Morishita, T. Mühlethaler, J. Lim, D. Ritz, P. S. Y. Long, P. A. Lehner, Z. H. Lim, M. Degen, Z. Yao, T. Maier, Y. Hou, J. Y. Lee, J. Xu, A. Y. J. Yeat, K. T. S. Koh, W. Y. Goh, S. Y. H. Ling, P. W. L. Chua, M. Yamazaki, P. L. R. Ee, S. Hiller, B. I. Morinaka, Antibiotics that kill gram-negative bacteria by restructuring the outer membrane protein BamA. bioRxiv 2024.12.16.628070 [Preprint] (2024). https://doi.org/10.1101/2024.12.16.628070.
73. X. Zhang, O. Lytovchenko, S. L. Lundstrom, R. A. Zubarev, M. Gaetani, Proteome Integral Solubility Alteration (PISA) assay in mammalian cells for deep, high-confidence, and high-throughput target deconvolution. *Bio Protoc.* **12**, e4556 (2022).
74. M. Gaetani, R. A. Zubarev, Proteome Integral Solubility Alteration (PISA) for high-throughput ligand target deconvolution with increased statistical significance and reduced sample amount. *Methods Mol. Biol.* **2554**, 91–106 (2023).
75. M. Choi, C. Y. Chang, T. Clough, D. Broudy, T. Killeen, B. MacLean, O. Vitek, MSstats: An R package for statistical analysis of quantitative mass spectrometry-based proteomic experiments. *Bioinformatics* **30**, 2524–2526 (2014).
76. G. W. Bemis, M. A. Murcko, The properties of known drugs. 1. Molecular frameworks. *J. Med. Chem.* **39**, 2887–2893 (1996).
77. A. E. Jerse, Experimental gonococcal genital tract infection and opacity protein expression in estradiol-treated mice. *Infect. Immun.* **67**, 5699–5708 (1999).
78. V. J. Savage, C. Charrier, A. M. Salisbury, H. Box, N. Chaffer-Malam, A. Huxley, R. Kirk, G. M. Noonan, S. Mohmed, M. W. Craighead, A. J. Ratcliffe, S. A. Best, N. R. Stokes, Efficacy of a novel tricyclic topoisomerase inhibitor in a murine model of *Neisseria gonorrhoeae* infection. *Antimicrob. Agents Chemother.* **60**, 5592–5594 (2016).
79. W. Jin, R. Barzilay, T. Jaakkola, Multi-objective molecule generation using interpretable substructures. arXiv:2002.03244 [cs.LG] (2020).
80. N. S. Ramadoss, J. N. Alumasa, L. Cheng, Y. Wang, S. Li, B. S. Chambers, H. Chang, A. K. Chatterjee, A. Brinker, I. H. Engels, K. C. Keiler, Small molecule inhibitors of trans-translation have broad-spectrum antibiotic activity. *Proc. Natl. Acad. Sci. U.S.A.* **110**, 10282–10287 (2013).

Acknowledgments: We thank A. Graveline, A. Vernet, and M. Sanchez Suarez for veterinary expertise and assistance; A. Kosaraju, L. Minall, and J. Vacca at Phare Bio for sharing data and insightful discussions; and A. Vrcic, B. Marion, and the Broad Institute CDoT team for HTS assistance, compound acquisition, and advice. **Funding:** This work was supported by the Defense Threat Reduction Agency, grant HDTRA-12210032 (J.J.C.); the National Institutes of Health (NIH), R01AI146194 (J.J.C.), K08AI182474 (M.N.A.), T32CA921641 (M.N.A.), R01AI132606 and R01AI153521 (S.G.P. and Y.H.G.), and K25AI168451 (F.W.); Broad Institute of MIT and Harvard (J.J.C.); Siebel Scholars Foundation (J.A.V.); MIT–Novo Nordisk Artificial Intelligence Postdoctoral Fellows Program (S.M.M.); Swiss National Science Foundation, grant SNSF_203071 (A.K.); Knut and Alice Wallenberg Foundation, grant KAW2022.0347 (A.L.); Swedish Research Council, grant 2023-02692 (A.A.S.); Bill and Melinda Gates Foundation (D.E.I.); and the Wyss Institute for Biologically Inspired Engineering at Harvard University (D.E.I.). This work is part of the Antibiotics-AI Project (J.J.C.) and supported by the Audacious Project, Flu Lab, LLC, the Sea Grape Foundation, Rosamund Zander and Hansjorg Wyss for the Wyss Foundation, and an anonymous donor. **Author contributions:** M.N.A., J.A.V., S.M.M., and J.J.C. conceptualized the paper and administered the project. M.N.A., S.M.M., A.K., S.G.P., E.J.Z., A.G., A. Jorgenson, A. Junaid, P.B., P.E., and Y.Z. designed and performed in vitro experiments. M.N.A. and N.M.D. designed and performed in vivo experiments. J.A.V., A.L., K.S., and F.W. performed computational analyses and contributed to methodology. S.M.M., D.R., M. Gaborieau, E.L., M. Gaetani, M.-S.A., and A.A.S. performed, supervised, and analyzed the mass spectrometry–based experiments. M.N.A, J.A.V., S.M.M., and A.K. visualized data. Y.H.G., D.E.I., and J.J.C. supervised the work. M.N.A., J.A.V., A.G., and J.J.C. wrote the original draft, and all authors reviewed and edited the manuscript. **Competing interests:** J.J.C. is a cofounder and scientific advisory board (SAB) chair of Phare Bio (a nonprofit venture focused on antibiotic drug development), academic cofounder and board member of Cellarity, and the founding SAB chair of Integrated Biosciences. M.N.A. is a cofounder and consultant to Day Zero Diagnostics. F.W. is a cofounder of Integrated Biosciences. Y.H.G. is on the SAB and clinical advisory board of Day Zero Diagnostics and on the SAB of Decoy Therapeutics. D.E.I. is founder, board member, and SAB chair of Emulate Inc. M.N.A., J.A.V., and J.J.C. are inventors on a patent application related to this work ("Discovery of antimicrobials using machine learning," US 63/683242). All other authors declare that they have no competing interests. **Data, code, and materials availability:** Proteomic data have been deposited to the ProteomeXchange Consortium (www.proteomexchange.org/) with identifiers PXD067530 and PXD067696 and the MassIVE partner repository (https://massive.ucsd.edu/) with identifier MSV000098897. All other data associated with this study are present in the paper or the Supplementary Materials, including data file S1. All code developed and used for this work can be found in the GitHub repository (https://github.com/jackievaleri/ngonorrhoeae_abx_ml_discovery), with the version of record on Zenodo (*54*). Associated models and data files are deposited in a separate, related record on Zenodo (*55*). The GCGS0759 strain was obtained from the CDC; requests for this strain should be directed to the CDC. Availability of the HHH023 strain is dependent on Division of Microbiology and Infectious Diseases, National Institute of Allergy and Infectious Diseases, approval. All other materials used or generated in this study are commercially available or will be supplied upon reasonable request.

Submitted 14 August 2024
Resubmitted 15 September 2025
Accepted 12 May 2026
Published 17 June 2026
10.1126/scitranslmed.ads4699

Science Translational Medicine

Deep learning–enabled discovery of antibiotics effective against *Neisseria gonorrhoeae*

Melis N. Anahtar, Jacqueline A. Valeri, Seyed Majed Modaresi, Aarti Krishnan, Nina M. Donghia, Samantha G. Palace, Erica J. Zheng, Aakanksha Gulati, Alicia Jorgenson, Abidemi Junaid, Parijat Bandyopadhyay, Andreas Luttens, Krishna Suresh, Paige Edwards, Felix Wong, Yu Zhang, Danilo Ritz, Margaux Gaborieau, Edmund Loh, Massimiliano Gaetani, Marie-Stephanie Aschtgen, Amir Ata Saei, Yonatan H. Grad, Donald E. Ingber, and James J. Collins

Sci. Transl. Med. **18** (854), eads4699. DOI: 10.1126/scitranslmed.ads4699

Editor's summary

Neisseria gonorrhoeae, a well-known cause of sexually transmitted disease, has grown increasingly treatment resistant, and identifying effective ways to tackle this pathogen is an utmost priority. Here, Anahtar *et al.* developed and validated a deep learning model before using it to explore chemical space for molecules predicted to inhibit *N. gonorrhoeae* growth. From their top hits, the authors chose for further testing two selective compounds with chemical structures different from known antibiotics that also showed in vitro efficacy against multidrug-resistant *N. gonorrhoeae* strains, low human cell cytotoxicity, and low resistance propensity. One compound showed efficacy against *N. gonorrhoeae* in a human tissue–mimicking vagina-on-a-chip model, and the other compound reduced bacterial load in an in vivo mouse model of vaginal *N. gonorrhoeae* infection. This study presents an informatic antibiotic discovery tool and enriches the stockpile of potential treatments to tackle gonococcal infection. —Catherine Charneski